Dalton Transactions

Cite this: *Dalton Trans.*, 2011, **40**, 11497

www.rsc.org/dalton

**PAPER**



# The oxidative conversion of the *N*,*S*-bridged complexes [{RhLL′(μ-X)}$_2$] to [(RhLL′)$_3$(μ-X)$_2$]$^+$ (X = mt or taz): a comparison with the oxidation of *N*,*N*-bridged analogues†

**Robin J. Blagg,‡ María J. López-Gómez,§ Jonathan P. H. Charmant, Neil G. Connelly,* John J. Cowell, Mairi F. Haddow, Alex Hamilton, A. Guy Orpen, Thomas Riis-Johannessen and Saowanit Saithong**

***Received 17th May 2011, Accepted 4th August 2011***
**DOI: 10.1039/c1dt10930h**

The structures of [{RhLL′(μ-X)}$_2$] [LL′ = cod, (CO)$_2$, (CO)(PPh$_3$) or {P(OPh)$_3$}$_2$; X = mt or taz], prepared from [{RhLL′(μ-Cl)}$_2$] and HX in the presence of NEt$_3$, depend on the auxiliary ligands LL′. The head-to-tail arrangement of the two *N*,*S*-bridges is accompanied by a rhodium-eclipsed conformation for the majority but the most hindered complex, [{Rh[P(OPh)$_3$]$_2$(μ-taz)}$_2$], uniquely adopts a sulfur-eclipsed structure. The least hindered complex, [{Rh(CO)$_2$(μ-mt)}$_2$], shows intermolecular stacking of mt rings in the solid state. The complexes [{RhLL′(μ-X)}$_2$] are chemically oxidised to trinuclear cations, [(RhLL′)$_3$(μ-X)$_2$]$^+$, most probably *via* reaction of one molecule of the dimer, in the sulfur-eclipsed form, with the fragment [RhLL′]$^+$ formed by oxidative cleavage of a second.

## Introduction

During our studies of the synthesis of the scorpionate complexes [RhL$_2$T*x*] {T*x* = hydrotris(methimazolyl)borate, Tm or HB(mt)$_3$;[1] T*x* = hydrotris(4-ethyl-3-methyl-5-thioxo-1,2,4-triazolyl)borate, Tt = HB(taz)$_3$ [2]}, from rhodium precursors such as [{RhL$_2$(μ-Cl)}$_2$] [L$_2$ = (CO)$_2$, cycloocta-1,5-diene (cod), *etc.*] and KT*x*, we occasionally observed the formation of small quantities of by-products, apparently dimers with the rhodium atoms bridged by *N*,*S*-donors originating from the T*x* anion. We have now directly synthesised and fully characterised these species as [{RhLL′(μ-X)}$_2$] (X = methimazolyl, mt or thioxotriazolyl, taz; Fig. 1), analogues of complexes with other *N*,*S*-bridges, *e.g.* pyridine-2-thiolate (pyt),[3–7] benzothiazole-2-thiolate (bzt),[3,4,8–10] 2-mercaptothiazolinate (mtz),[5,11] benzimidazole-2-thiolate (Hbzimt),[12,13] pyridine-2,6-dithiolate[14] and ω-thiocaprolactamate,[6] showing how the bridging and ancillary ligands affect molecular conformation. In addition, we describe their reactions with chemical one-electron oxidants, providing a new route to trinuclear [(RhLL′)$_3$(μ-X)$_2$]$^+$ rather than to paramagnetic monocations [{RhLL′(μ-X)}$_2$]$^+$ analogous to those isolated from the oxidation of *N*,*N*-bridged species such as [{Rh(CO)(PPh$_3$)(μ-X)}$_2$] (X = *p*-tolNNNtol-*p*[15] or 2-*t*-butylpyrazolyl[16]).

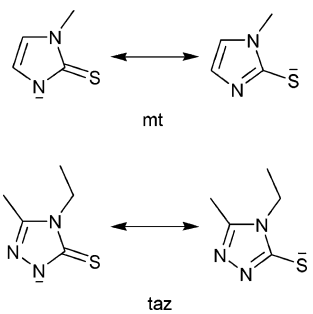


**Fig. 1** Bridging *N*,*S*-donating heterocycles.

## Results and discussion

### Synthesis and characterisation of dirhodium(I) methimazolyl and thioxotriazolyl complexes

The complexes [{Rh(cod)(μ-X)}$_2$] (X = mt, **1** or taz, **2**) were obtained by reacting [{Rh(cod)(μ-Cl)}$_2$] with methimazole, Hmt, in $CH_2Cl_2$ or with thioxotriazole, Htaz, in toluene to give [Rh(cod)Cl(HX)] and then deprotonating the coordinated heterocycle using triethylamine. The dimers were then isolated by either evaporating the reaction mixture to dryness and subsequent extraction into toluene, for **1**, or direct removal of the precipitated salt [NEt$_3$H]Cl for **2**. In both cases, the yellow or orange solid

*School of Chemistry, University of Bristol, Bristol, BS8 1TS, UK. E-mail: Neil.Connelly@bristol.ac.uk; Tel: +44(0)117 9288162*

† Electronic supplementary information (ESI) available: X-ray structures of **1**, **2**, **6** and **12**$^+$[BF$_4$]$^-$·$CH_2Cl_2$; $^{13}$C-{$^1$H} NMR spectroscopic data for **2**, **4**, **6**, **7**, **9**$^+$[PF$_6$]$^-$, **11**$^+$[PF$_6$]$^-$ and **13**$^+$[PF$_6$]$^-$. CCDC reference numbers 826255–826265. For ESI and crystallographic data in CIF or other electronic format see DOI: 10.1039/c1dt10930h

‡ Current address: Department of Chemistry, The University of Manchester, Oxford Road, Manchester, M13 9PL, UK. E-mail: robin.blagg@manchester.ac.uk

§ Current address: UCR-CNRS Joint Research Chemistry Laboratory, Department of Chemistry, University of California, Riverside, CA 92521-0403, USA. E-mail: maria@ucr.edu

was isolated by concentrating the toluene solution and adding *n*-hexane.

The preparation of [{Rh(CO)$_2$(μ-mt)}$_2$] **3** from [{Rh(CO)$_2$(μ-Cl)}$_2$], Hmt and NEt$_3$ was similar to that of **1**, the red toluene extract giving a dark blue-brown solid on treatment with *n*-hexane. In this case the IR spectrum of the initial mixture of [{Rh(CO)$_2$(μ-Cl)}$_2$] and Hmt in $CH_2Cl_2$ showed two strong bands of equal intensity at 2080 and 2011 cm$^{-1}$, evidence for the monomeric intermediate *cis*-[Rh(CO)$_2$Cl(Hmt)]. Using a similar method to synthesise [{Rh(CO)$_2$(μ-taz)}$_2$] **4** was unsuccessful, although *cis*-[Rh(CO)$_2$Cl(Htaz)] was observed by IR spectroscopy {$\nu$(CO) = 2084, 2014 cm$^{-1}$} following initial bridge cleavage of [{Rh(CO)$_2$(μ-Cl)}$_2$]. However, the tetracarbonyl **4** was synthesised in good yield by bubbling CO through a $CH_2Cl_2$ solution of **2**, thereby substituting the cod ligands.

The bis(phosphine) derivative [{Rh(CO)(PPh$_3$)(μ-mt)}$_2$] **5** was prepared from [{Rh(CO)$_2$(μ-mt)}$_2$] **3** and two equivalents of PPh$_3$ in toluene but attempts to prepare the monosubstituted complex, by adding only one equivalent of PPh$_3$, gave a mixture of [Rh$_2$(CO)$_3$(PPh$_3$)(μ-mt)$_2$] {$\nu$(CO) = 2061, 1994(br) cm$^{-1}$}, the dimer **5** and unreacted tetracarbonyl **3**. (The complex [Rh$_2$(CO)$_3$(PPh$_3$)(μ-bzt)$_2$] {$\nu$(CO) (in Nujol) = 2065, 1997, 1995 cm$^{-1}$} has been structurally characterised in the solid state but exists in equilibrium with [{Rh(CO)$_2$(μ-bzt)}$_2$] and [{Rh(CO)(PPh$_3$)(μ-bzt)}$_2$] in solution.[9]) The analogue [{Rh(CO)(PPh$_3$)(μ-taz)}$_2$] **6** was synthesised by an alternative route, namely by reacting [{Rh(CO)(PPh$_3$)(μ-Cl)}$_2$] with Htaz in $CH_2Cl_2$, to give [Rh(CO)Cl(PPh$_3$)(Htaz)] {$\nu$(CO) = 1979 cm$^{-1}$} which was deprotonated using triethylamine.

Finally, the tetrakis(phosphite) complex [{Rh[P(OPh)$_3$]$_2$(μ-taz)}$_2$] **7** was synthesised from **4** and an excess of P(OPh)$_3$. In order to ensure complete carbonyl substitution, the reaction mixture was stirred for 80 min and then evaporated to dryness *in vacuo*. After extraction into toluene, filtration and precipitation by adding *n*-hexane, the complex was further purified by chromatography on a silica/$CH_2Cl_2$ column. A single yellow band was eluted with $CH_2Cl_2$ and the product, **7**, precipitated using *n*-hexane.

Complexes **1–7** (Scheme 1) were characterised by elemental analysis, IR and NMR spectroscopy (Table 1) and, in all cases except **4**, by X-ray crystallography.

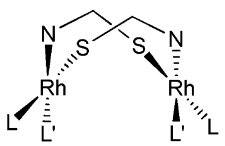


| | N^S | L, L' |
|---|---|---|
| **1** | mt | cod |
| **2** | taz | cod |
| **3** | mt | CO, CO |
| **4** | taz | CO, CO |
| **5** | mt | CO, PPh$_3$ |
| **6** | taz | CO, PPh$_3$ |
| **7** | taz | P(OPh)$_3$, P(OPh)$_3$ |

**Scheme 1** Dirhodium complexes.

The IR spectra in the carbonyl region of [{Rh(CO)$_2$(μ-mt)}$_2$] **3** {$\nu$(CO) = 2080(s), 2059(m), 2011(s) cm$^{-1}$} and [{Rh(CO)$_2$(μ-taz)}$_2$] **4** {$\nu$(CO) = 2086(s), 2062(m), 2019(s) cm$^{-1}$} are very similar, each showing three bands (but with a shoulder, at *ca.* 2010 cm$^{-1}$, discernible on the lowest energy band of **4**). The reported spectra of other complexes with *N*,*S*-bridging ligands, with similar molecular structures (see below), are surprisingly variable in the number and energy of the bands observed, *e.g.* [{Rh(CO)$_2$(μ-pyt)}$_2$] {$\nu$(CO) = 2080(vs), 2055(s), 2015(vs), 1980(w) cm$^{-1}$}[3] and [{Rh(CO)$_2$(μ-mtz)}$_2$] {$\nu$(CO) = 2094(s), 2058(m), 2045(w, sh), 2018(s) cm$^{-1}$},[11] though the spectrum of the *N*,*N*-bridged pyrazolyl complex [{Rh(CO)$_2$(μ-pz)}$_2$] {pz = pyrazolyl; $\nu$(CO) = 2090, 2079, 2021 cm$^{-1}$}[17] appears to be more like those of **3** and **4**. The observation of two closely spaced IR bands {$\nu$(CO) = 1974, 1967 cm$^{-1}$} for [{Rh(CO)(PPh$_3$)(μ-mt)}$_2$] **5**, as in [{Rh(CO)(PPh$_3$)(μ-bzt)}$_2$],[3] is consistent with the arrangement of the carbonyl ligands determined crystallographically (see below); only one broad, unresolved band was observed for [{Rh(CO)(PPh$_3$)(μ-taz)}$_2$] **6** {ν(CO) = 1975 cm$^{-1}$} and [{Rh(CO)(PPh$_3$)(μ-mtz)}$_2$] {$\nu$(CO) = 1981 cm$^{-1}$}.[11]

**NMR spectroscopy and fluxional behaviour.** Proton and $^{31}$P NMR spectroscopic data for complexes **1–7** are given in Table 1. (Representative $^{13}$C-{$^1$H} NMR spectroscopic data, for the taz complexes **2**, **4**, **6** and **7**, are given in the ESI.†) The two bridging ligands in each of [{Rh(cod)(μ-mt)}$_2$] **1** and [{Rh(cod)(μ-taz)}$_2$] **2** are equivalent (for example, the ring methyl substituents appear as only one singlet). Likewise, in each complex the two cod rings are equivalent although the eight carbon atoms in each ring are inequivalent. Thus, at −80 (for **1**) or −60 °C (for **2**) four peaks are observed for the alkene protons or carbons of the cod ligand, as seen for [{Rh(cod)(μ-Hbzimt)}$_2$].[12] (The $^1$H signals for the cod ligands of **1** and **2** are very broad at room temperature, probably as a result of rotation of the cod ligand about the metal-cod axis.[5])

In contrast to **1** and **2**, both the $^1$H and $^{13}$C-{$^1$H} spectra of the tetracarbonyl [{Rh(CO)$_2$(μ-taz)}$_2$] **4** (but not [{Rh(CO)$_2$(μ-mt)}$_2$] **3**) show the presence of two isomers, **4a** and **4b**, in a 3 : 2 ratio {*e.g.* four doublets are observed for the rhodium-bound carbonyls, two for **4a**, at 187.64 ($^1J_{CRh}$ 64.5 Hz) and 182.86 ($^1J_{CRh}$ 69.1 Hz) and two for **4b**, at 186.14 ($^1J_{CRh}$ 66.2 Hz) and 185.05 ($^1J_{CRh}$ 68.0 Hz)}. The major spectral differences are the lower chemical shifts for the resonances of **4a**, the observation of two diastereotopic methylene protons for each thioxotriazolyl ethyl group of **4a**, and the greater difference between the chemical shifts of the two carbonyl carbons for **4a** {$\Delta(\delta_C)$ 4.78 ppm} compared with **4b** {$\Delta(\delta_C)$ 1.09 ppm}. Such significant differences suggest a mixture of 'head-to-tail' and 'head-to-head' isomers. (Resolution was insufficient in $CH_2Cl_2$ to detect the isomers by IR spectroscopy in the carbonyl region.) Why **4** should appear as a mixture of isomers while the precursor, **2**, does not is unknown. The tetracarbonyl may undergo isomerisation more readily than the cod complex though we have no evidence to support or disprove this.

The protons of the thioxotriazolyl rings of [{Rh[P(OPh)$_3$]$_2$(μ-taz)}$_2$] **7** were generally observed at low chemical shifts due to the shielding effect of the twelve P(OPh)$_3$ phenyl rings which surround the Rh(μ-taz)$_2$Rh core. The tendency for nearby aromatic rings to shift the resonances of protons on the thioxotriazolyl ring (especially the terminal protons of the ethyl group) has been observed in [Rh(CO)(PPh$_3$)Tt][2] and [Rh(CO)(PPh$_3$){HB(taz)$_2$(pz$^{Ph}$)}][18] at

 

**Table 1** Analytical and spectroscopic data for dimeric rhodium complexes

| Complex | Colour | Yield/% | Analysis/%[a] | | | IR/cm$^{-1}$ | NMR[c] | |
|---|---|---|---|---|---|---|---|---|
| | | | C | H | N | $\nu$(CO)[b] | $^1$H | $^{31}$P-{$^1$H} |
| [{Rh(cod)(μ-mt)}$_2$] **1** | Yellow | 92 | 44.4 (44.5) | 5.1 (5.3) | 8.5 (8.6) | — | 6.51 (d, 2H, $^3J_{HH}$ 1.6, mt 4/5-*H*), 6.39 (d, 2H, $^3J_{HH}$ 1.6, mt 4/5-*H*), 4.78 (br m, 2H, cod C*H*), 4.08 (br m, 2H, cod C*H*), 3.75 (br m, 2H, cod C*H*), 3.70 (br m, 2H, cod C*H*), 3.28 (s, 6H, mt 3-C$H_3$), 2.65 (br m, 2H, cod CH$H^{exo}$), 2.50 (br m, 2H, cod CH$H^{exo}$), 2.29 (br m, 4H, cod CH$H^{exo}$), 1.93 (br m, 2H, cod CH$H^{endo}$), 1.74 (br m, 6H, cod CH$H^{endo}$)[d] | — |
| [{Rh(cod)(μ-taz)}$_2$] **2** | Orange | 93 | 42.2 (42.5)[e] | 5.8 (5.5) | 11.2 (11.2) | — | 4.80 (br m, 2H, cod C*H*), 4.12 (br m, 2H, cod C*H*), 3.98 (br m, 2H, cod C*H*), 3.72 (br m, 2H, cod C*H*), 3.64 (q, 4H, $^3J_{HH}$ 7.0, taz 4-C$H_2$CH$_3$), 2.76–2.13 (br m, 8H, cod CH$H^{exo}$), 2.04 (s, 6H, taz 3-C$H_3$), 1.98–1.54 (br m, 8H, cod CH$H^{endo}$), 1.03 (t, 6H, $^3J_{HH}$ 7.0, taz 4-CH$_2$C$H_3$)[f] | — |
| [{Rh(CO)$_2$(μ-mt)}$_2$] **3** | Blue-brown | 77 | 26.1 (26.5) | 2.1 (1.9) | 10.5 (10.3) | 2080, 2059(m), 2011 | 6.47 (d, 2H, $^3J_{HH}$ 1.7, mt 4/5-*H*), 6.39 (d, 2H, $^3J_{HH}$ 1.7, mt 4/5-*H*), 3.33 (s, 6H, mt 3-C$H_3$) | — |
| [{Rh(CO)$_2$(μ-taz)}$_2$] **4** | Purple | 64 | 28.0 (27.9) | 3.0 (2.7) | 14.0 (14.0) | 2086, 2062(m), 2019, 2010(sh) | 3.93 (dq, 2H, $^2J_{HH}$ 14.2, $^3J_{HH}$ 7.2, taz 4-CH*H*CH$_3$)[†], 3.93 (q, 4H, $^3J_{HH}$ 7.3, taz 4-C$H_2$CH$_3$)[‡], 3.74 (dq, 2H, $^2J_{HH}$ 14.2, $^3J_{HH}$ 7.2, taz 4-CH*H*CH$_3$)[†], 2.29 (s, 6H, taz 3-C$H_3$)[‡], 2.18 (s, 6H, taz 3-C$H_3$)[†], 1.24 (t, 6H, $^3J_{HH}$ 7.3, taz 4-CH$_2$C$H_3$)[‡], 1.14 (t, 6H, $^3J_{HH}$ 7.2, taz 4-CH$_2$C$H_3$)[†][g] | — |
| [{Rh(CO)(PPh$_3$)(μ-mt)}$_2$] **5** | Yellow | 32 | 54.8 (54.5) | 4.4 (4.0) | 5.0 (5.5) | 1974, 1967 | 7.78–6.58 (m, 30H, P*Ph*$_3$), 5.81 (d, 2H, $^3J_{HH}$ 1.6, mt 4/5-*H*), 5.27 (d, 2H, $^3J_{HH}$ 1.6, mt 4/5-*H*), 2.55 (s, 6H, mt 3-C$H_3$)[h] | 41.38 (d, $^1J_{PRh}$ 161, *P*Ph$_3$)[g] |
| [{Rh(CO)(PPh$_3$)(μ-taz)}$_2$] **6** | Yellow | 43 | 53.6 (53.8) | 4.2 (4.3) | 8.0 (7.9) | 1975(brd) | 7.71–7.15 (m, 30H, P*Ph*$_3$), 3.37 (dq, 2H, $^2J_{HH}$ 13.7, $^3J_{HH}$ 6.8, taz 4-C*H*HCH$_3$) 3.28 (dq, 2H, $^2J_{HH}$ 13.7, $^3J_{HH}$ 6.8, taz 4-CH*H*CH$_3$), 1.77 (s, 6H, taz 3-C$H_3$), 0.80 (t, 6H, $^3J_{HH}$ 7.0, taz 4-CH$_2$C$H_3$) | 41.98 (d, $^1J_{PRh}$ 162, *P*Ph$_3$) |
| [{Rh[P(OPh)$_3$]$_2$(μ-taz)}$_2$] **7** | Yellow | 22 | 56.0 (55.9)[e] | 4.5 (4.4) | 4.6 (4.7) | — | 7.35–6.78 {m, 60H, P(O*Ph*)$_3$}, 3.23 (dq, 2H, $^2J_{HH}$ 14.3, $^3J_{HH}$ 7.3, taz 4-C*H*HCH$_3$) 2.64 (dq, 2H, $^2$J$_{HH}$ 14.1, $^3J_{HH}$ 7.2, taz 4-CH*H*CH$_3$), 1.79 (s, 6H, taz 3-C$H_3$), 0.41 (t, 6H, $^3J_{HH}$ 7.3, taz 4-CH$_2$C$H_3$) | 127.83 {dd, $^1J_{PRh}$ 265, $^2J_{PP}$ 70, *P*(OPh)$_3$}, 115.99 {dd, $^1J_{PRh}$ 265, $^2J_{PP}$ 70, *P*(OPh)$_3$} |

[a] Calculated values in parentheses. [b] In $CH_2Cl_2$; strong absorptions unless stated, m = medium, sh = shoulder, brd = broad. [c] Chemical shift ($\delta$) in ppm, $J$ values in Hz, spectra in $CD_2Cl_2$ at 20 °C unless otherwise stated. [d] At −80 °C. [e] Calculated as a 2 : 1 $CH_2Cl_2$ solvate. [f] At −60 °C. [g] Two isomers present in a ratio of 3[†]:2[‡]. [h] In $d_8$-toluene.

low temperature and [{Rh(CO)($PPh_3$)(μ-taz)}$_2$] **6** at room temperature.

The $^{31}$P-{$^1$H} NMR spectra of **5** and **6** each show only one doublet (at *ca.* 42 ppm, $J_{PRh}$ 160 Hz), consistent with the presence of only one (head-to-tail) isomer in which two equivalent phosphorus atoms are each coupled to rhodium; [{Rh(CO)($PPh_3$)(μ-mtz)}$_2$] similarly showed a single doublet, at 39.81 ($J_{PRh}$ 164 Hz) ppm.[11] The tetrakis(phosphite) [{Rh[P(OPh)$_3$]$_2$(μ-taz)}$_2$] **7** shows two doublets of doublets, at 127.83 and 115.99 ($J_{PRh}$ 265, $^2J_{PP}$ 70 Hz) ppm, again consistent with only one isomer in which, however, the two phosphites on each metal are inequivalent (one is *trans* to N and the other to S).

**The X-ray structures of complexes 1–3 and 5–7.** In order to determine the relative orientations of the two heterocyclic bridges in the new dimers (*i.e.* head-to-head or head-to-tail), and to define more fully the effects of the bridging and ancillary ligands on conformation, X-ray diffraction studies were carried out on [{Rh(cod)(μ-mt)}$_2$] **1**, [{Rh(cod)(μ-taz)}$_2$] **2**, [{Rh(CO)$_2$(μ-mt)}$_2$]·toluene **3**·toluene, [{Rh(CO)($PPh_3$)(μ-mt)}$_2$]·toluene **5**·toluene, [{Rh(CO)($PPh_3$)(μ-taz)}$_2$] **6** and [{Rh[P(OPh)$_3$]$_2$(μ-taz)}$_2$]·$CH_2Cl_2$ **7**·$CH_2Cl_2$ using crystals grown by slow diffusion of *n*-hexane into a concentrated toluene (for **1**, **3** and **5**) or $CH_2Cl_2$ (for **2**, **6** and **7**) solution of each complex at 5 °C. The structures of **2**, **3**, **5** and **7** are shown in Fig. 2–5 as representative examples (those of **1** and **6** are shown in the ESI†) with selected bond lengths and angles for all six species in Table 2.

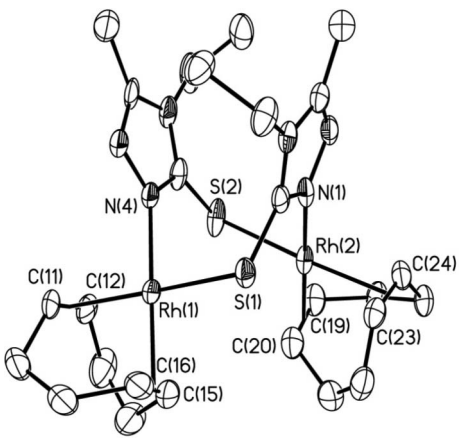


**Fig. 2** Molecular structure of [{Rh(cod)(μ-taz)}$_2$] **2**. (One of two inequivalent molecules in the unit cell; the second is shown in the ESI†. In this and all other structures reported in this paper, ellipsoids are shown at the 50% probability level and hydrogen atoms are omitted for clarity.)

All of the complexes **1–3**, **5** and **6** have an 'open book' geometry in which the two heterocycles bridge two *cis* positions of slightly distorted square planar $d^8$ metals. (The structure of **7** is very different, see below.) Overall, the complexes have approximate $C_2$ rotational symmetry, *i.e.* a $C_2$ axis runs between the ring planes, through the middle of the Rh-N-C-S-Rh-N-C-S eight-membered ring.

In each complex, the two rings bridge head-to-tail so that each rhodium atom is *cis* *N*,*S*-coordinated. In both $PPh_3$ complexes, **5** and **6**, the phosphine ligands are *trans* to the sulfur atoms, *i.e.* the site of carbonyl substitution in **3** or **4** depends on the higher *trans* effect of the sulfur donor. (The tendency of $PPh_3$ to coordinate to rhodium *trans* to sulfur rather than nitrogen has also been observed in [{Rh(CO)($PPh_3$)(μ-pyt)}$_2$] [6] and [{Rh(CO)($PPh_3$)(μ-mtz)}$_2$].[11]) The mutually *trans* arrangement of the two phosphine ligands (across the P–Rh···Rh–P unit) also minimises steric hindrance.

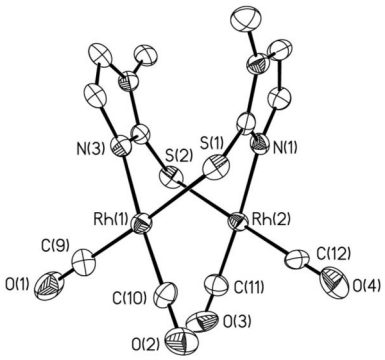


**Fig. 3** Molecular structure of [{Rh(CO)$_2$(μ-mt)}$_2$] **3**.

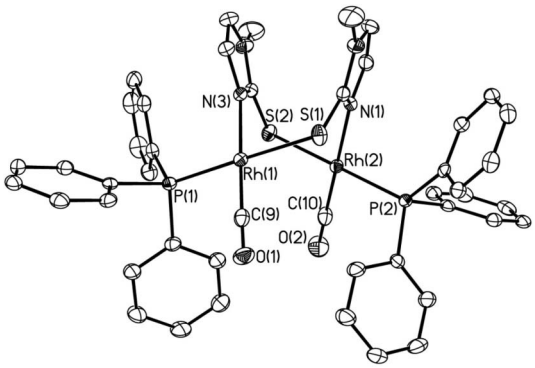


**Fig. 4** Molecular structure of [{Rh(CO)($PPh_3$)(μ-mt)}$_2$] **5**.

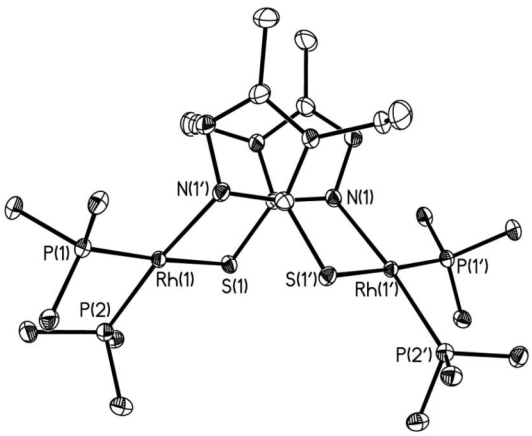


**Fig. 5** Molecular structure of [{Rh{P(OPh)$_3$}$_2$(μ-taz)}$_2$] **7** (phenyl rings omitted for clarity).

The coordination planes of the two metals are inclined, at an angle $\theta$, and twisted, by an angle $\beta$ (the average of the two S–Rh···Rh–N dihedral angles, Table 2); the combined inclination and twisting minimises steric repulsion between the ancillary ligands, particularly cod or $PPh_3$. In the dicarbonyl [{Rh(CO)$_2$(μ-mt)}$_2$] **3**, $\theta$ is 20.7° but in the cod complexes **1** and **2** (which has two independent but essentially isostructural molecules in the unit

 

**Table 2** Selected bond lengths (Å) and angles (°) for dimeric rhodium complexes

| | [{Rh(cod)-(μ-mt)}$_2$] **1** | [{Rh(cod)-(μ-taz)}$_2$] **2**[a] | [{Rh(CO)$_2$-(μ-mt)}$_2$] **3** | [{Rh(CO)(PPh$_3$)-(μ-mt)}$_2$] **5** | [{Rh(CO)(PPh$_3$)-(μ-taz)}$_2$] **6** | [{Rh[P(OPh)$_3$]$_2$-(μ-taz)}$_2$] **7**[b] |
|---|---|---|---|---|---|---|
| Rh(1)···Rh(2) | 3.847(1) | 3.832(1), 3.893(1) | 3.049(1) | 3.618(1) | 3.651(1) | 4.968(1) |
| Rh(1)–X(1)[c] {X(1)–O} | 2.003(2) | 1.996(7), 1.966(6) | 1.851(6) {1.152(7)} | 2.274(1) | 2.261(1) | 2.161(1) |
| Rh(1)–X(2)[d] {X(2)–O} | 2.011(2) | 2.011(7), 2.007(6) | 1.858(6) {1.129(6)} | 1.817(2) {1.149(3)} | 1.826(4) {1.148(4)} | 2.163(1) |
| Rh(1)–S(1) | 2.364(1) | 2.362(2), 2.351(2) | 2.382(1) | 2.383(1) | 2.394(1) | 2.408(1) |
| Rh(1)–N($z$)[e] {X(3)–O} | 2.096(2) | 2.086(5), 2.080(5) | 2.097(4) {1.125(7)} | 2.088(2) | 2.084(4) | 2.087(2) |
| Rh(2)–X(3)[f] {X(4)–O} | 2.017(2) | 2.003(7), 1.997(8) | 1.874(6) {1.140(6)} | 2.266(1) | 2.258(1) | — |
| Rh(2)–X(4)[g] | 2.007(3) | 2.006(7), 2.002(6) | 1.848(6) | 1.817(2) {1.149(3)} | 1.817(4) {1.146(4)} | — |
| Rh(2)–S(2) | 2.360(1) | 2.360(2), 2.350(2) | 2.381(1) | 2.378(1) | 2.395(1) | — |
| Rh(2)–N(1) | 2.093(2) | 2.087(5), 2.069(5) | 2.086(4) | 2.089(2) | 2.079(3) | — |
| S(1)···S(2) | 4.493(1) | 4.496(3), 4.543(2) | 4.770(2) | 4.638(2) | 4.662(2) | 3.776(1) |
| X(1)–Rh(1)–X(2) | 87.90(8) | 88.20(3), 88.09(2) | 92.5(2) | 89.70(7) | 89.27(11) | 91.75(2) |
| S(1)–Rh(1)–N($z$) | 91.69(5) | 91.73(13), 91.30(13) | 88.65(12) | 88.91(5) | 87.95(8) | 89.26(5) |
| X(3)–Rh(2)–X(4) | 88.63(7) | 87.94(3), 87.66(3) | 91.8(2) | 88.01(8) | 89.03(12) | — |
| S(2)–Rh(2)–N(1) | 90.75(5) | 91.36(13), 92.22(14) | 88.49(12) | 89.28(5) | 88.62(8) | — |
| S(1)–Rh(1)···Rh(2)–N(1) | –42.35(5) | –43.17(14), –39.73(15) | –31.63(12) | –42.16(5) | 38.10(9) | 59.85(6) |
| S(2)–Rh(2)···Rh(1)–N($z$) | –40.82(5) | –42.53(15), –41.77(13) | –31.09(12) | –42.60(5) | 38.29(8) | — |
| $\theta$[h] | 52.7 | 51.2, 54.3 | 20.7 | 46.9 | 46.1 | 86.0 |
| $\beta$[i] | –41.6 | –41.8 | –31.4 | –42.3 | 38.2 | 59.9 |
| ring$_{centroid}$–ring$_{centroid}$ | 3.445 | 3.466, 3.514 | 3.485 | 3.354 | 3.165 | 3.129 |

[a] Two independent molecules in the unit cell. [b] Molecular structure $C_2$ symmetric, other bond lengths/angles equivalent by symmetry. In this structure, Rh(2) = Rh(1′). [c] X(1) = midpoint C(9)–C(10) **1**; midpoint C(11)–C(12) **2**; C(9) **3**; P(1) **5**–**7**. [d] X(2) = midpoint C(13)–C(14) **1**; midpoint C(15)–C(16) **2**; C(10) **3**; C(9) **5**; C(11) **6**; P(2) **7**. [e] N($z$) = N(3) **1**, **3** and **5**; N(4) **2** and **6**; N(1′) **7**. [f] X(3) = midpoint C(21)–C(22) **1**; midpoint C(23)–C(24) **2**; C(12) **3**; P(2) **5** and **6**. [g] X(4) = midpoint C(17)–C(18) **1**; midpoint C(19)–C(20) **2**; C(11) **3**; C(10) **5**; C(12) **6**. [h] $\theta$ = angle between the planes {Rh(1), X(1), X(2), S(1), N($z$)} and {Rh(2), X(3), X(4), S(2), N(1)}. [i] $\beta$ = average of the S(1)–Rh(1)···Rh(2)–N dihedral angles.

cell, **2a** and **2b**) and the carbonyl phosphine analogues **5** and **6** that angle is much larger, at 46.1–54.3°. Likewise, $\beta$ varies from 31.4° in dicarbonyl **3** to *ca*. 42° in the cod complexes **1** and **2**.

In all cases the Rh···Rh distance is too long to indicate significant metal-metal interaction. However, it is affected significantly by the nature of the ancillary ligands, increasing from 3.05 Å in the tetracarbonyl **3** to 3.62 and 3.65 Å in the carbonyl phosphines **5** and **6** and to *ca*. 3.85 Å in the cod complexes **1** and **2**. Surprisingly, these distances are significantly longer than those reported for analogous *N*,*S*-bridged complexes such as [{Rh(CO)$_2$(μ-pyt)}$_2$] {2.941(2) Å}[3] (*cf*. **3**), [{Rh(CO)(PPh$_3$)(μ-pyt)}$_2$] {3.195(1) Å}[6] and [{Rh(CO)(PPh$_3$)(μ-mtz)}$_2$] {3.244(1)Å}[11] (*cf*. **5** and **6**) and [{Rh(cod)(μ-mtz)}$_2$] {3.715(1) Å}[5] (*cf*. **1** and **2**).

One other observation is of interest in this series of dimers, namely that solid **3** is much darker (blue-brown), and with a metallic aspect, than **1**, **2** and **5**–**7** (yellow or orange). (The other new tetracarbonyl, **4**, was isolated as a purple powder rather than a crystalline solid, possibly due to the presence of isomers, so has not been structurally characterised. Note that all of **1**–**7** are yellow or orange in solution.) However, the crystal structure of **3** (Fig. 6) is also unique in that the dimers are linked *via* intermolecular π-stacking of methimazolyl rings. The rings in adjacent dimers are parallel, though offset (by *ca*. 0.9 Å) from being perfectly eclipsed, with a distance between the ring centroids of 3.78 Å. (This distance compares with the intramolecular ring$_{centroid}$–ring$_{centroid}$ distances of 3.17–3.51 Å in **1**, **2**, **5** and **6**, Table 2.) Presumably, the sterically more demanding cod and PPh$_3$ ligands of **1**, **2**, **5** and **6** prevent such stacking in the solid state. It is interesting to note that [{Rh(CO)$_2$(μ-pyt)}$_2$] was described as dichroic green-purple in the solid state. Its molecular structure has been reported but no comment was made on any stacking in the crystal structure.[3] Further inspection of the original crystallographic data showed that neither the relative orientation of the pyridyl rings nor their intermolecular ring$_{centroid}$–ring$_{centroid}$ distance indicated such stacking.

As noted above, the structure of [{Rh[P(OPh$_3$)]$_2$(μ-taz)}$_2$] **7** is distinctly different from those of the other new dimers. In this case, and presumably because of the presence of four sterically demanding phosphite ligands, the two rhodium square planes are approximately mutually perpendicular ($\theta$ = 86°) and twisted by

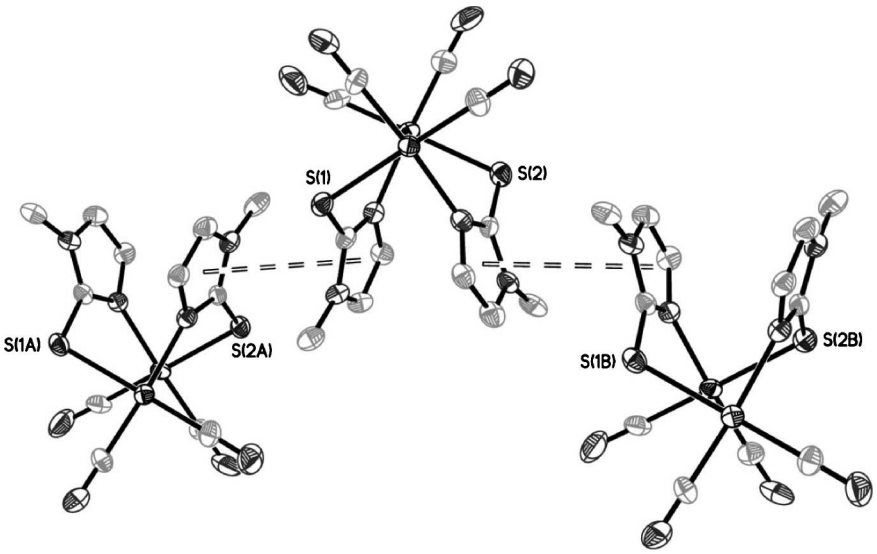


**Fig. 6** π-Stacking between the methimazolyl rings in [{Rh(CO)$_2$(μ-mt)}$_2$] **3**. Symmetry operator for symmetry-generated atoms: A: $x$, 0.5 – $y$, –0.5 + $z$. B: $x$, 0.5 – $y$, 0.5 + $z$.

*ca*. 60°. Accordingly, the rhodium–rhodium distance is increased to 4.97 Å. However, the sulfur–sulfur distance is decreased to 3.78 Å (*cf*. 4.49–4.77 Å in **1–6**) and, overall, **7** uniquely adopts a sulfur-eclipsed 'twist-tub' conformation of the eight-membered Rh-N-C-S-Rh-N-C-S ring [Fig. 7(a)] (*cf*. the rhodium-eclipsed conformation in **1–3**, **5** and **6** [Fig. 7(b)]).

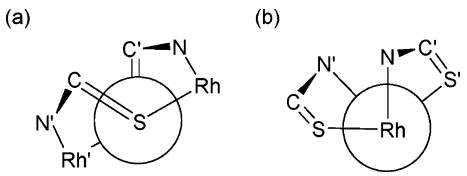


**Fig. 7** (a) The sulfur-eclipsed 'twist-tub' conformation of the Rh-N-C-S-Rh-N-C-S ring of **7**, and (b) the rhodium-eclipsed 'twist-tub' conformation of that ring in **1–3**, **5** and **6**.

**The electrochemistry of complexes 1–7.** The cyclic voltammograms of **1–7** in $CH_2Cl_2$ are rather poorly defined relative to those of *N*,*N*-bridged species such as [{Rh(CO)(PPh$_3$)(μ-X)}$_2$] (X = *p*-tolNNNtol-*p*[15] or 2-*t*-butylpyrazolyl[16]) which are reversibly oxidised to stable monocations. However, all of the new dimers do show chemically accessible oxidation processes (Table 3) (some with further ill-defined oxidation at more positive potentials). The cod complex [{Rh(cod)(μ-mt)}$_2$] **1** shows an apparently chemically reversible wave centred at 0.32 V, implying some stability for the cation [{Rh(cod)(μ-mt)}$_2$]$^+$. However, the oxidations of **2** [{Rh(cod)(μ-taz)}$_2$], and the carbonyl phosphine complexes **6** and **7**, are only partially reversible, the reversibility increasing with scan rate, *e.g.* the peak current ratio for **6** increases from *ca.* 0.4 at 50 mV s$^{-1}$ to *ca.* 0.6 at 1.0 V s$^{-1}$. The instability of the *N*,*S*-bridged monocations of **1–7** is therefore in marked contrast to the stability of the structurally characterised monocations formed from the *N*,*N*-bridged triazenide and pyrazolyl complexes noted above. Given the reactions described below, one might speculate that rapid Rh-S bond cleavage occurs after the formation of **1**$^+$–**7**$^+$.

**Table 3** Electrochemical data for the oxidation of dimeric rhodium complexes[a]

| | $(E_p)_{ox}$/V | $(E_p)_{red}$/V | $E^{\circ\prime}$/V | $(i_p)_{red}/(i_p)_{ox}$ |
|---|---|---|---|---|
| [{Rh(cod)(μ-mt)}$_2$] **1** | 0.38 | 0.26 | 0.32[b] | 1.0 |
| [{Rh(cod)(μ-taz)}$_2$] **2** | 0.55 | 0.39 | 0.47 | 0.40 |
| [{Rh(CO)$_2$(μ-mt)}$_2$] **3** | 0.68 | — | — | — |
| [{Rh(CO)$_2$(μ-taz)}$_2$] **4** | 0.42[c] | — | — | — |
| [{Rh(CO)(PPh$_3$)(μ-mt)}$_2$] **5** | 0.28 | — | — | — |
| [{Rh(CO)(PPh$_3$)(μ-taz)}$_2$] **6** | 0.36 | 0.28 | 0.32 | 0.52 |
| [{Rh[P(OPh)$_3$]$_2$(μ-taz)}$_2$] **7** | 0.50 | 0.36 | 0.43 | 0.74 |

[a] CV at a platinum disc electrode at scan rate, 200 mV s$^{-1}$. Calibrated *vs.* [Fe(η-C$_5$Me$_5$)$_2$]$^{0/1+}$ at $E^{\circ\prime}$ = –0.08 V. [b] Second, irreversible, wave with $(E_p)_{ox}$ = 0.75 V. [c] Broad, ill-defined wave.

The oxidation of the tetrakis(phosphite) complex [{Rh[P(OPh)$_3$]$_2$(μ-taz)}$_2$] **7** appears surprisingly positive compared with those of [{Rh(CO)$_2$(μ-taz)}$_2$] **4** and [{Rh(CO)(PPh$_3$)(μ-mt)}$_2$] **6** in that carbonyl substitution by *P*-donors usually leads to considerably lower potentials (*cf.* the triazenide complexes [{RhL$_2$(μ-PhNNNPh)}$_2$] {L$_2$ = (CO)$_2$, 0.88 V; (CO)(PPh$_3$), 0.56 V; (PPh$_3$)$_2$, 0.22 V}[19]). However, as shown above, this complex is structurally unique in the series **1–7** so that direct comparison is difficult.

Finally, cyclic voltammetry provides further evidence for stepwise phosphine substitution in the carbonyl [{Rh(CO)$_2$(μ-mt)}$_2$] **3**. After adding one equivalent of PPh$_3$ to **3** in $CH_2Cl_2$ the irreversible oxidation wave at *ca*. 0.70 V is replaced by three peaks, at *ca*. 0.74, 0.44 and 0.32 V, possibly corresponding to the oxidation of a mixture of [{Rh(CO)$_2$(μ-mt)}$_2$] **3**, [Rh$_2$(CO)$_3$(PPh$_3$)(μ-mt)$_2$] and [{Rh(CO)(PPh$_3$)(μ-mt)}$_2$] **5** respectively. After the addition of two equivalents of PPh$_3$, only two irreversible waves are observed, at *ca*. 0.30 and 0.75 V, probably corresponding first to the oxidation of **5**, to give [{Rh(CO)(PPh$_3$)(μ-mt)}$_2$]$^+$, and then of the product of a rapid following chemical reaction, possibly [{Rh(CO)(PPh$_3$)}$_3$(μ-mt)$_2$]$^+$ (see below).

 

### Synthesis and characterisation of $[(RhLL')_3(\mu\text{-}X)_2]^+$

The observation by cyclic voltammetry of chemically accessible oxidation processes, albeit mostly ill-defined, led us to investigate the reactions of $[\{RhLL'(\mu\text{-}X)\}_2]$ **1–7** with one-electron oxidants. Rather than leading to the paramagnetic monocations $[\{RhLL'(\mu\text{-}X)\}_2]^+$, as found for $[\{Rh(CO)(PPh_3)(\mu\text{-}X)\}_2]$ (X = *p*-tolNNNtol-*p*[15] or 2-*t*-butylpyrazolyl[16]), a new route was discovered to trinuclear cations of the type $[(RhLL')_3(\mu\text{-}X)_2]^+$.

Treatment of **1**, **3** or **5** in $CH_2Cl_2$ with two equivalents of $[Fe(\eta\text{-}C_5H_4COMe)(\eta\text{-}C_5H_5)][BF_4]$, or of **2**, **4** or **6** with $[Fe(\eta\text{-}C_5H_5)_2][PF_6]$, resulted in colour changes from yellow or orange to deep red or purple and the isolation, on addition of *n*-hexane, of red-purple solids characterised as the trinuclear salts $[\{Rh(cod)\}_3(\mu\text{-}mt)_2][BF_4]$ **8**$^+[BF_4]^-$, $[\{Rh(cod)\}_3(\mu\text{-}taz)_2][PF_6]$ **9**$^+[PF_6]^-$, $[\{Rh(CO)_2\}_3(\mu\text{-}mt)_2][BF_4]$ **10**$^+[BF_4]^-$, $[\{Rh(CO)_2\}_3(\mu\text{-}taz)_2][PF_6]$ **11**$^+[PF_6]^-$, $[\{Rh(CO)(PPh_3)\}_3(\mu\text{-}mt)_2][BF_4]$ **12**$^+[BF_4]^-$ and $[\{Rh(CO)(PPh_3)\}_3(\mu\text{-}taz)_2][PF_6]$ **13**$^+[PF_6]^-$.

Yields of $[\{Rh(CO)_2\}_3(\mu\text{-}taz)_2][PF_6]$ **11**$^+[PF_6]^-$ were poor by this method but the dark purple solid was obtained more readily by bubbling CO through **9**$^+[PF_6]^-$ in $CH_2Cl_2$. By contrast, similar carbonylation of **8**$^+[BF_4]^-$ led to the isolation of the novel species $[Rh_3(CO)_4(cod)(\mu\text{-}mt)_2][BF_4]$ **14**$^+[BF_4]^-$. IR spectroscopy showed that all three cod ligands were first replaced by CO, giving **10**$^+$, but five minutes after gas passage was stopped the carbonyl groups on the central rhodium atom had been substituted by the displaced cod, giving a purple solution with IR carbonyl bands at 2080 and 2026 cm$^{-1}$. Adding *n*-hexane to the mixture, and storage at −10 °C, gave purple crystals of **14**$^+[BF_4]^-$ (which is also formed when an excess of cod is added to pure **10**$^+$ in $CH_2Cl_2$). (Reversible diene substitution was also observed between CO and $[\{Rh(cod)\}_3(\mu\text{-}pyt)_2]^+$.[4])

Although pure $[(Rh\{P(OPh)_3\}_2)_3(\mu\text{-}taz)_2][PF_6]$ could not be isolated, spectroscopic evidence was obtained for its formation by two distinct synthetic routes. First, the $^{31}P\text{-}\{^1H\}$ NMR spectrum of the crude solid formed by oxidising **7** with $[Fe(\eta\text{-}C_5H_5)_2][PF_6]$ in $CH_2Cl_2$ showed the presence of $[(Rh\{P(OPh)_3\}_2)_3(\mu\text{-}taz)_2]^+$ (six separate doublets of doublets: 125.52 $\{^1J_{PRh}$ 199, $^2J_{PP}$ 61$\}$, 123.43 $\{^1J_{PRh}$ 258, $^2J_{PP}$ 69$\}$, 111.83 $\{^1J_{PRh}$ 304, $^2J_{PP}$ 69$\}$, 109.26 $\{^1J_{PRh}$ 304, $^2J_{PP}$ 73$\}$, 92.99 $\{^1J_{PRh}$ 191, $^2J_{PP}$ 52$\}$, 88.01 $\{^1J_{PRh}$ 181, $^2J_{PP}$ 62$\}$) as well as unreacted **7**. Second, the $^{31}P\text{-}\{^1H\}$ NMR spectrum of the product of the reaction of a large excess of $P(OPh)_3$ with $[\{Rh(CO)_2\}_3(\mu\text{-}taz)_2][PF_6]$ **11**$^+[PF_6]^-$ in $CH_2Cl_2$ suggested the presence of both $[(Rh\{P(OPh)_3\}_2)_3(\mu\text{-}taz)_2][PF_6]$ and partially substituted products, *i.e.* $[Rh_3\{P(OPh)_3\}_x(CO)_{6-x}(\mu\text{-}taz)_2][PF_6]$, also indicated by new carbonyl bands in the IR spectrum of the crude solid.

Complexes **8**$^+$–**13**$^+$ (Scheme 2) were characterised as $[BF_4]^-$ or $[PF_6]^-$ salts by elemental analysis, IR and NMR spectroscopy (Table 4) and, for **9**$^+$, **10**$^+$ and **12**$^+$–**14**$^+$, by X-ray crystallography. (Representative $^{13}C\text{-}\{^1H\}$ NMR spectroscopic data, for the taz complexes **9**$^+$, **11**$^+$ and **13**$^+$, are given in the ESI.†)

Four IR carbonyl bands were observed for each of the hexacarbonyls $[\{Rh(CO)_2\}_3(\mu\text{-}mt)_2][BF_4]$, **10**$^+[BF_4]^-$, and $[\{Rh(CO)_2\}_3(\mu\text{-}taz)_2][PF_6]$, **11**$^+[PF_6]^-$, and two each for **12**$^+$–**14**$^+$, (closely spaced for **12**$^+$ and **13**$^+$, containing $Rh(CO)(PPh_3)$ units, and well separated for the *cis*-dicarbonyl units in **14**$^+$). These spectra are comparable with those of analogous *N*,*S*-bridged trirhodium complexes such as $[\{Rh(CO)_2\}_3(\mu\text{-}bzt)_2]^+$ $\{\nu(CO)$ = 2088(vs), 2055(s), 2020(vs) cm$^{-1}\}$ and $[\{Rh(CO)(PPh_3)\}_3(\mu\text{-}bzt)_2]^+$ $\{\nu(CO)$ = 2000 cm$^{-1}\}$[4] though, again, previously reported spectra are surprisingly variable in the number and energy of the bands observed.

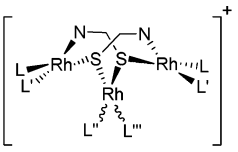


| | N⌒S | L, L' | L'', L''' |
|---|---|---|---|
| **8**$^+$ | mt | cod | cod |
| **9**$^+$ | taz | cod | cod |
| **10**$^+$ | mt | CO, CO | CO, CO |
| **11**$^+$ | taz | CO, CO | CO, CO |
| **12**$^+$ | mt | CO, $PPh_3$ | CO, $PPh_3$ |
| **13**$^+$ | taz | CO, $PPh_3$ | CO, $PPh_3$ |
| **14**$^+$ | mt | CO, CO | cod |

**Scheme 2** Trirhodium cations.

The $^1H$ NMR spectra show the two bridging heterocycles to be equivalent in **8**$^+$–**11**$^+$ and **14**$^+$ but not in the carbonyl phosphine complexes **12**$^+$ or **13**$^+$ because of the two different ancillary ligands on each metal. Thus, $[\{Rh(CO)(PPh_3)\}_3(\mu\text{-}mt)_2]^+$ **12**$^+$ gives four peaks for the alkene protons of the mt rings and two for the two methyl substituents. The cations $[\{Rh(cod)\}_3(\mu\text{-}X)_2]^+$ (X = mt, **8**$^+$ or taz, **9**$^+$) each showed six signals for the alkene protons and carbons of the three cod rings, corresponding to four distinct environments on each of the terminal $[Rh(cod)]^+$ centres and two on the central $[Rh(cod)]^+$ fragment (as also found for this fragment in $[Rh_3(CO)_4(cod)(\mu\text{-}mt)_2]^+$ **14**$^+$). Six $^{13}C$ resonances are also observed for the alkane carbons of the cod rings of **9**$^+$ (see the ESI†). However, in all of **8**$^+$, **9**$^+$ and **14**$^+$ the hydrocarbon ligand signals are broad at room temperature, suggesting slow rotation about the metal-cod axis, as in the dimers **1** and **2**.

The room temperature NMR spectra of $[\{Rh(CO)_2\}_3(\mu\text{-}taz)_2]^+$ **11**$^+$ are well defined with, for example, all three carbonyl environments (*trans*-S–*cis*-S, *trans*-N–*cis*-S and *trans*-S–*cis*-N) observed as rhodium-coupled $^{13}C$ doublets (183.98, 183.84 and 180.66 ppm; $^1J_{CRh}$ 68.0 Hz). Both $[\{Rh(CO)(PPh_3)\}_3(\mu\text{-}mt)_2]^+$ **12**$^+$ and $[\{Rh(CO)(PPh_3)\}_3(\mu\text{-}taz)_2]^+$ **13**$^+$ show three distinct signals in the $^{31}P\text{-}\{^1H\}$ NMR spectrum, each a doublet with coupling to rhodium, as found for the analogous *N*,*S*-bridged complex $[\{Rh(CO)(PPh_3)\}_3(\mu\text{-}bzt)_2]^+$.[4] The two thioxotriazolyl rings are magnetically inequivalent, the proton and carbon resonances at lower chemical shifts for one ring possibly resulting from different degrees of shielding from the aromatic rings of the $PPh_3$ ligands.

Other trinuclear complexes with *N*,*S*-bridging units have been prepared[4,8] by adding a reactive fragment, $[RhLL']^+$, to an *N*,*S*-bridged dimer, *e.g.* $[\{Rh(CO)_2\}_3(\mu\text{-}pyt)_2]^+$ from $[Rh(CO)_2(acetone)_n]^+$ and $[\{Rh(CO)_2(\mu\text{-}pyt)\}_2]$.[4] It is therefore proposed that oxidation of $[\{RhLL'(\mu\text{-}X)\}_2]$ (**1–7**) results in bridge cleavage, the liberated fragment $[RhLL']^+$ *S*-coordinating to a second molecule of $[\{RhLL'(\mu\text{-}X)\}_2]$ to give $[(RhLL')_3(\mu\text{-}X)_2]^+$ (**8**$^+$–**14**$^+$). However, for such coordination to take place the rhodium-eclipsed geometry of **1–6** must convert to the sulfur-eclipsed form (as found in **7**), as shown in Scheme 3.

**The electrochemistry of complexes 8$^+$–13$^+$.** For completeness, a brief electrochemical study was made of the trinuclear species **8**$^+$–**13**$^+$ (Table 5). Again, the cod complexes showed chemically

**Table 4** Analytical and spectroscopic data for cationic trirhodium complexes

| Complex | Colour | Yield/% | Analysis/%[a] | | | IR/cm$^{-1}$ | NMR[c] | |
|---|---|---|---|---|---|---|---|---|
| | | | C | H | N | $\nu$(CO)[b] | $^{1}$H | $^{31}$P-{$^{1}$H} |
| [{Rh(cod)}$_3$(μ-mt)$_2$]-[BF$_4$] **8**$^+$[BF$_4$]$^-$ | Purple | 34 | 40.5 (40.6) | 4.9 (4.9) | 6.0 (5.9) | — | 6.64 (d, 2H, $^3J_{HH}$ 2.0, mt 4/5-*H*), 6.24 (d, 2H, $^3J_{HH}$ 2.0, mt 4/5-*H*), 5.55–5.45 (br m, 2H, cod C*H*), 5.35–5.35 (br m, 1H, cod C*H*), 4.95–4.80 (br m, 2H, cod C*H*), 4.65–4.55 (br m, cod C*H*), 4.50–4.35 (br m, 2H, cod C*H*), 4.25–4.15 (br m, 2H, cod C*H*), 3.92 (s, 6H mt 3-C$H_3$), 3.40–3.30 (br m, 2H, cod C*H*), 3.25–2.75 (m, 6H, cod C$H_2$), 2.70–1.95 (m, 12H, cod C$H_2$), 1.90–1.55 (m, 6H, cod C$H_2$) | — |
| [{Rh(cod)}$_3$(μ-taz)$_2$]-[PF$_6$] **9**$^+$[PF$_6$]$^-$ | Dark red | 49 | 38.2 (38.4) | 5.0 (4.9) | 8.0 (7.9) | — | 5.63–5.54 (br m, 2H, cod C*H*), 4.93–5.05 (br m, 2H, cod C*H*), 4.90–4.81 (br m, 2H, cod C*H*), 4.83 (dq, 2H, $^2J_{HH}$ 14.5, $^3J_{HH}$ 7.3, taz 4-C*H*HCH$_3$), 4.63–4.52 (br m, 2H, cod C*H*), 4.29–4.21 (br m, 2H, cod C*H*), 4.07 (dq, 2H, $^2J_{HH}$ 14.6, $^3J_{HH}$ 7.3, taz 4-CH*H*CH$_3$), 3.51–3.40 (br m, 2H, cod C*H*), 3.23–2.76 (m, 6H, cod C$H_2$), 2.61–2.12 (m, 12H, cod C$H_2$), 2.14 (s, 6H, taz 3-C$H_3$), 1.98–1.69 (m, 6H, cod C$H_2$), 1.63 (t, 6H, $^3J_{HH}$ 7.3, taz 4-CH$_2$C$H_3$) | — |
| [{Rh(CO)$_2$}$_3$(μ-mt)$_2$]-[BF$_4$] **10**$^+$[BF$_4$]$^-$ | Red-orange | 6 | 21.4 (21.3) | 1.7 (1.3) | 7.0 (7.1) | 2109(ms), 2091(s), 2046(s,brd), 2035 (sh) | 6.95 (d, 2H, $^3J_{HH}$ 1.6, mt 4/5-*H*), 6.66 (d, 2H, $^3J_{HH}$ 1.6, mt 4/5-*H*), 3.62 (s, 6H, mt 3-C$H_3$) | — |
| [{Rh(CO)$_2$}$_3$(μ-taz)$_2$]-[PF$_6$] **11**$^+$[PF$_6$]$^-$ | Dark purple | 64 | 21.3 (21.2) | 2.0 (1.8) | 9.1 (9.3) | 2109, 2088, 2049, 2030(m) | 4.04 (q, 2H, $^3J_{HH}$ 7.3, taz 4-C$H_2$CH$_3$), 4.03 (q, 2H, $^3J_{HH}$ 7.3, taz 4-C$H_2$CH$_3$), 2.45 (s, 6H, taz 3-C$H_3$), 1.21 (t, 6H, $^3J_{HH}$ 7.3, taz 4-CH$_2$C$H_3$) | — |
| [{Rh(CO)(PPh$_3$)}$_3$(μ-mt)$_2$][BF$_4$] **12**$^+$[BF$_4$]$^-$ | Pink | 9 | 54.2 (52.3) | 3.9 (3.7) | 3.3 (3.8) | 2003, 1990 | 7.74–7.10 (m, 45H, P*Ph*$_3$), 6.02 (s, 1H, mt 4/5-*H*), 5.86 (s, 1H, mt 4/5-*H*), 5.35 (s, 1H, mt 4/5-*H*), 5.34 (s, 1H, mt 4/5-*H*), 3.53 (s, 3H, mt 3-C$H_3$), 3.27 (s, 3H, mt 3-C$H_3$) | 40.03 (d, $^1J_{PRh}$ 167, *P*Ph$_3$), 39.61 (d, $^1J_{PRh}$ 166, *P*Ph$_3$), 38.17 (d, $^1J_{PRh}$ 154, *P*Ph$_3$) |
| [{Rh(CO)(PPh$_3$)}$_3$(μ-taz)$_2$][PF$_6$] **13**$^+$[PF$_6$]$^-$ | Dark red | 12 | 46.4 (46.6)[d] | 3.8 (3.7) | 5.0 (4.7) | 2005, 1995 | 7.77–7.14 (m, 45H, P*Ph*$_3$), 4.34 (dq, 1H, $^2J_{HH}$ 14.7, $^3J_{HH}$ 7.3, taz 4-C*H*HCH$_3$), 4.12 (dq, 1H, $^2J_{HH}$ 14.4, $^3$J$_{HH}$ 7.2, taz 4-C*H*HCH$_3$), 3.60 (dq, 1H, $^2J_{HH}$ 14.5, $^3J_{HH}$ 7.0, taz 4-CH*H*CH$_3$), 3.41 (dq, 1H, $^2J_{HH}$ 14.6, $^3J_{HH}$ 7.5, taz 4-CH*H*CH$_3$), 1.54 (s, 6H, taz 3-C$H_3$), 1.21 (t, 3H, $^3J_{HH}$ 7.1, taz 4-CH$_2$C$H_3$), 1.02 (t, 3H, $^3J_{HH}$ 7.3, taz 4-CH$_2$C$H_3$) | 40.35 (d, $^1J_{PRh}$ 169, *P*Ph$_3$), 39.89 (d, $^1J_{PRh}$ 168, *P*Ph$_3$), 39.31 (d, $^1J_{PRh}$ 154, *P*Ph$_3$), -143.91 (septet, $^1J_{PF}$ 710, *P*F$_6$) |
| [Rh$_3$(CO)$_4$(cod)(μ-mt)$_2$]-[BF$_4$] **14**$^+$[BF$_4$]$^-$ | Purple | 80 | 29.3 (28.5) | 3.1 (2.6) | 6.5 (6.7) | 2080, 2026 | 6.84 (br s, 2H, mt 4/5-*H*), 6.54 (br s, 2H, mt 4/5-*H*), 5.25–5.15 (br m, 2H, cod C*H*), 3.95–3.75 (br m, 2H, cod C*H*), 3.56 (s, 6H, mt 3-C$H_3$), 3.00–2.85 (br m, 2H, cod CH*H*$^{exo}$), 2.55–2.40 (br m, 2H, cod CH*H*$^{exo}$), 2.35–2.25 (br m, 2H, cod CH*H*$^{endo}$), 2.00–1.80 (br m, 2H, cod CH*H*$^{endo}$) | — |

[a] Calculated values in parentheses. [b] In $CH_2Cl_2$; strong (s) absorptions unless stated, m = medium, sh = shoulder, brd = broad. [c] Chemical shift ($\delta$) in ppm, $J$ values in Hz, spectra in $CD_2Cl_2$ at 20 °C. [d] Calculated as a 1 : 2 $CH_2Cl_2$ solvate.

 

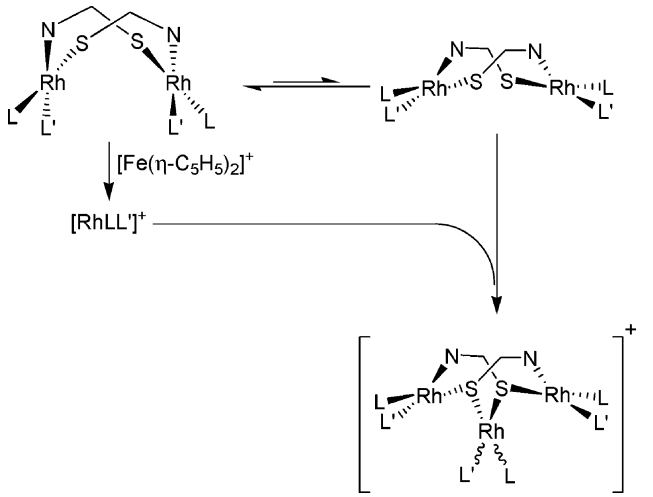


**Scheme 3**

reversible ($\mathbf{8}^+$) or near reversible ($\mathbf{9}^+$) oxidation waves but at much more positive potentials than those of the analogous dimers **1** and **2**. As with the dimers, the hexacarbonyl cations are the least stable on oxidation.

**The X-ray structures of complexes $\mathbf{9}^+$, $\mathbf{10}^+$ and $\mathbf{12}^+$–$\mathbf{14}^+$.** In order to define their structures more fully, X-ray diffraction studies were carried out on crystals of $[\{Rh(cod)\}_3(\mu\text{-taz})_2][PF_6]$ $\mathbf{9}^+[PF_6]^-$, $[\{Rh(CO)_2\}_3(\mu\text{-mt})_2][BF_4]$ $\mathbf{10}^+[BF_4]^-$, $[\{Rh(CO)(PPh_3)\}_3(\mu\text{-mt})_2][BF_4]\cdot CH_2Cl_2$ $\mathbf{12}^+[BF_4]^-\cdot CH_2Cl_2$, $[\{Rh(CO)(PPh_3)\}_3(\mu\text{-taz})_2][PF_6]\cdot 3CH_2Cl_2$ $\mathbf{13}^+[PF_6]^-\cdot 3CH_2Cl_2$ and $[Rh_3(CO)_4(cod)(\mu\text{-mt})_2]$ $[BF_4]\cdot 2CH_2Cl_2$ $\mathbf{14}^+[BF_4]^-\cdot 2CH_2Cl_2$, grown by slow diffusion of *n*-hexane into a concentrated $CH_2Cl_2$ solution of each complex at 5 °C. The structures of $\mathbf{9}^+$, $\mathbf{10}^+$, $\mathbf{13}^+$ and $\mathbf{14}^+$ are shown in Fig. 8–11 as representative examples, with selected bond lengths and angles for all in Table 6. (The structure of $\mathbf{12}^+$ is shown in the ESI†.)

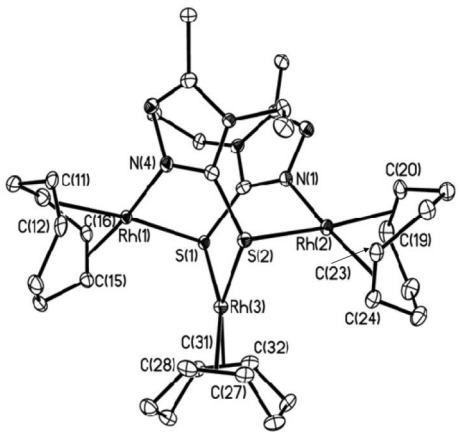


**Fig. 8** Structure of the cation $[\{Rh(cod)\}_3(\mu\text{-taz})_2]^+$ $\mathbf{9}^+$.

The trirhodium skeleton in each of $\mathbf{9}^+$, $\mathbf{10}^+$ and $\mathbf{12}^+$–$\mathbf{14}^+$ is bent with Rh···Rh···Rh angles (104.5–112.3°) comparable with those in $[\{Rh(CO)_2\}_3(\mu\text{-pyt})_2]^+$ [4] and $[Rh_2(cod)_2(\mu\text{-bzt})_2Ag(O_2ClO_2)]$[8] (112.7 and 110.5° respectively). The three rhodium atoms are linked by two rings, each of which is *N*-bonded to one terminal rhodium atom and *S*-bonded to both the other terminal and the central rhodium atoms. Thus, the end rhodium atoms are *cis N*,*S*-bound with minimal distortion from square planar geometry, as in the dimers **1–7**, while the central metal has a more distorted square planar arrangement with the two *cis*-bound sulfur atoms displaced from the RhLL′ plane.

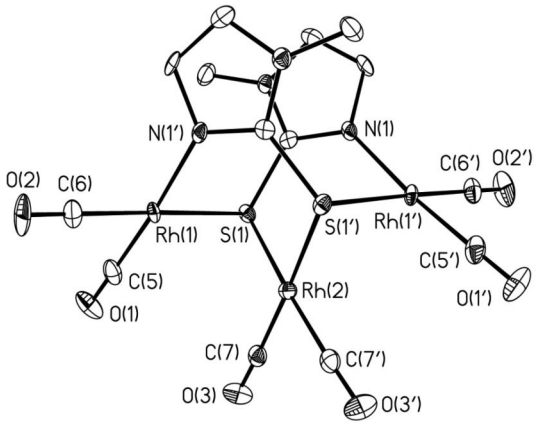


**Fig. 9** Structure of the cation $[\{Rh(CO)_2\}_3(\mu\text{-mt})_2]^+$ $\mathbf{10}^+$.

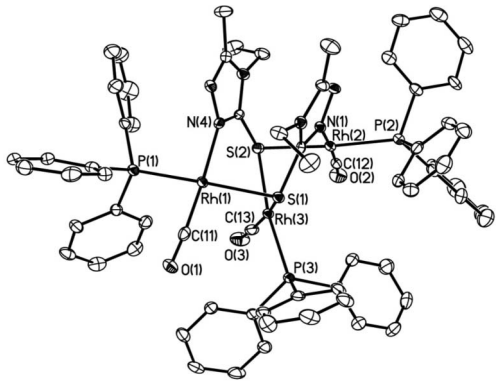


**Fig. 10** Structure of the cation $[\{Rh(CO)(PPh_3)\}_3(\mu\text{-taz})_2]^+$ $\mathbf{13}^+$.

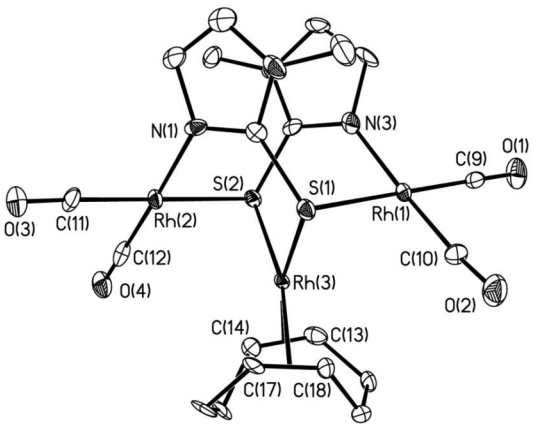


**Fig. 11** Structure of the cation $[Rh_3(CO)_4(cod)(\mu\text{-mt})_2]^+$ $\mathbf{14}^+$.

To form the trinuclear cations from the dimers **1–6**, the rhodium-eclipsed geometry of the Rh-N-C-S-Rh-N-C-S eight-membered ring distorts to the sulfur-eclipsed conformation (as observed in the structure of **7**) to accommodate the third metal. The terminal rhodium atoms move apart (*i.e.* compared with their positions in the parent dimer) so that, for example, Rh(2)···Rh(2)′ in $[\{Rh(CO)_2\}_3(\mu\text{-mt})_2]^+$ $\mathbf{10}^+$ is 5.076(2) Å and Rh(1)···Rh(2) in $[Rh(CO)(PPh_3)\}_3(\mu\text{-mt})_2]^+$ $\mathbf{12}^+$ is 5.062(1) Å, longer than 3.049(1)

**Table 5** Electrochemical data for the oxidation of cationic trirhodium complexes[a]

| | $(E_p)_{ox}$/V | $(E_p)_{red}$/V | $E^{\circ\prime}$/V | $(i_p)_{red}/(i_p)_{ox}$ |
|---|---|---|---|---|
| $[\{Rh(cod)\}_3(\mu\text{-mt})_2][BF_4]$ **8**$^+[BF_4]^-$ | 0.92 | 0.84 | 0.88[b] | 1.0 |
| $[\{Rh(cod)\}_3(\mu\text{-taz})_2][PF_6]$ **9**$^+[PF_6]^-$ | 1.01 | 0.91 | 0.97 | 0.83 |
| $[\{Rh(CO)_2\}_3(\mu\text{-mt})_2][BF_4]$ **10**$^+[BF_4]^-$ | 1.30 | — | — | — |
| $[\{Rh(CO)_2\}_3(\mu\text{-taz})_2][PF_6]$ **11**$^+[PF_6]^-$ | 1.08 | — | — | — |
| $[\{Rh(CO)(PPh_3)\}_3(\mu\text{-mt})_2][BF_4]$ **12**$^+[BF_4]^-$ | 0.80 | — | — | — |
| $[\{Rh(CO)(PPh_3)\}_3(\mu\text{-taz})_2][PF_6]$ **13**$^+[PF_6]^-$[c] | 0.81 | 0.69 | 0.75 | 0.96 |

[a] CV at a platinum disc electrode at scan rate, 200 mV $s^{-1}$. Calibrated *vs.* $[Fe(\eta\text{-}C_5H_5)_2]^{0/1+}$ at $E^{\circ\prime} = 0.47$ V unless stated. [b] Second, irreversible, wave with $(E_p)_{ox} = 1.32$ V. [c] Calibrated *vs.* $[Fe(\eta\text{-}C_5Me_5)_2]^{0/1+}$ at $E^{\circ\prime} = -0.08$ V.

**Table 6** Selected bond lengths (Å) and angles (°) for cationic trirhodium complexes

| | $[\{Rh(cod)\}_3(\mu\text{-taz})_2]^+$ **9**$^+$ | $[\{Rh(CO)_2\}_3(\mu\text{-mt})_2]^+$ **10**$^+$[a] | $[\{Rh(CO)(PPh_3)\}_3(\mu\text{-mt})_2]^+$ **12**$^+$ | $[\{Rh(CO)(PPh_3)\}_3(\mu\text{-taz})_2]^+$ **13**$^+$ | $[Rh_3(CO)_4(cod)(\mu\text{-mt})_2]^+$ **14**$^+$ |
|---|---|---|---|---|---|
| Rh(1)···Rh(2) | 5.205(1) | 5.076(2) | 5.062(1) | 5.019(2) | 5.042(2) |
| Rh(1)···Rh(3) | 3.291(1) | 3.055(1) | 3.077(1) | 3.137(1) | 3.047(1) |
| Rh(2)···Rh(3) | 3.292(1) | — | 3.034(1) | 3.120(1) | 3.073(2) |
| Rh(1)–X(1)[b] {X(1)–O} | 2.016(3) | 1.903(7) {1.123(9)} | 2.265(2) | 2.278(1) | 1.882(13) {1.120(15)} |
| Rh(1)–X(2)[c] {X(2)–O} | 2.022(3) | 1.872(8) {1.123(10)} | 1.835(9) {1.130(9)} | 1.834(5) {1.156(5)} | 1.873(11) {1.128(15)} |
| Rh(1)–N(*z*)[d] | 2.085(3) | 2.071(6) | 2.087(6) | 2.090(3) | 2.058(11) |
| Rh(1)–S(1) | 2.399(1) | 2.382(2) | 2.406(2) | 2.433(1) | 2.412(3) |
| Rh(2)–X(3)[e] {X(3)–O} | 2.021(4) | — | 2.261(2) | 2.287(1) | 1.875(12) {1.133(15)} |
| Rh(2)–X(4)[f] {X(4)–O} | 2.038(4) | — | 1.815(8) {1.144(9)} | 1.838(4) {1.144(5)} | 1.871(13) {1.124(16)} |
| Rh(2)–N(1) | 2.083(3) | — | 2.103(6) | 2.093(3) | 2.084(10) |
| Rh(2)–S(2) | 2.388(1) | — | 2.410(2) | 2.434(1) | 2.398(3) |
| Rh(3)–X(5)[g] {X(5)–O} | 2.032(3) | 1.864(8) {1.147(9)} | 2.272(2) | 1.846(5) {1.144(5)} | 2.047(10) |
| Rh(3)–X(6)[h] {X(6)–O} | 2.032(4) | — | 1.830(8) {1.137(8)} | 2.288(1) | 2.055(10) |
| Rh(3)–S(1) | 2.358(1) | 2.406(2) | 2.392(2) | 2.404(2) | 2.374(3) |
| Rh(3)–S(2) | 2.349(1) | — | 2.403(2) | 2.423(1) | 2.377(3) |
| S(1)···S(2) | 3.517(1) | 3.610(4) | 3.561(3) | 3.651(2) | 3.560(5) |
| Rh(1)···Rh(3)···Rh(2) | 104.49(1) | 112.34(3) | 111.86(2) | 106.68(1) | 110.92(4) |
| X(1)–Rh(1)–X(2) | 87.4(1) | 90.5(3) | 90.7(3) | 86.90(13) | 90.6(5) |
| S(1)–Rh(1)–N(*z*) | 91.54(9) | 88.93(15) | 88.61(17) | 88.47(10) | 90.0(3) |
| X(3)–Rh(2)–X(4) | 87.0(1) | — | 94.2(3) | 92.71(13) | 89.5(5) |
| S(2)–Rh(2)–N(1) | 89.61(9) | — | 89.07(17) | 88.10(10) | 89.3(3) |
| X(5)–Rh(3)–X(6) | 87.0(1) | 89.6(4) | 86.9(2) | 86.68(14) | 86.9(5) |
| S(1)–Rh(3)–S(2) | 96.70(3) | 97.20(9) | 95.92(6) | 98.30(4) | 97.00(11) |
| S(1)–Rh(1)···Rh(2)–N(1) | 62.6(1) | 57.6(2) | −56.0(2) | −65.00(12) | 60.7(3) |
| S(2)–Rh(2)···Rh(1)–N(*z*) | 64.4(1) | — | −61.23(19) | −67.50(12) | 58.3(3) |
| $\beta$[i] | 63.5 | 57.6 | −58.6 | −66.3 | 59.5 |
| $\theta(1)$[j] | 69.2 | 80.9 | 84.2 | 86.6 | 83.1 |
| $\theta(2)$[k] | 83.8 | 82.1 | 75.4 | 77.1 | 76.1 |
| $\theta(3)$[l] | 86.0 | — | 72.0 | 78.1 | 76.9 |
| $ring_{centroid}$–$ring_{centroid}$ | 3.704 | 3.291 | 3.259 | 3.204 | 3.280 |

[a] Molecular structure $C_2$ symmetric, other bond lengths/angles equivalent by symmetry. In this structure, Rh(3) = Rh(1′). [b] X(1) = midpoint C(11)–C(12) **9**$^+$; C(6) **10**$^+$; P(1) **12**$^+$ and **13**$^+$; C(9) **14**$^+$. [c] X(2) = midpoint C(15)–C(16) **9**$^+$; C(5) **10**$^+$; C(1) **12**$^+$; C(11) **13**$^+$; C(10) **14**$^+$. [d] N(*z*) = N(4) **9**$^+$ and **13**$^+$; N(1′) **10**$^+$; N(3), **12**$^+$ and **14**$^+$. [e] X(3) = midpoint C(19)–C(20) **9**$^+$; P(2) **12**$^+$ and **13**$^+$; C(11) **14**$^+$. [f] X(4) = midpoint C(23)–C(24) **9**$^+$; C(2) **12**$^+$; C(12) **13**$^+$; C(12) **14**$^+$. [g] X(5) = midpoint C(27)–C(28) **9**$^+$; C(7) **10**$^+$; P(3) **12**$^+$; C(13) **13**$^+$; midpoint C(13)–C(14) **14**$^+$. [h] X(6) = midpoint C(31)–C(32) **9**$^+$; C(3) **12**$^+$; P(3) **13**$^+$; midpoint C(17)–C(18) **14**$^+$. [i] $\beta$ = average of the S(1)–Rh(1)···Rh(2)–N dihedral angles. [j] $\theta(1)$ = angle between the planes {Rh(1), X(1), X(2), S(1), N(*z*)} and {Rh(2), X(3), X(4), S(2), N(1)}. [k] $\theta(2)$ = angle between the planes {Rh(3), X(5), X(6), S(1), S(2)} and {Rh(1), X(1), X(2), S(1), N(*z*)}. [l] $\theta(3)$ = angle between the planes {Rh(3), X(5), X(6), S(1), S(2)} and {Rh(2), X(3), X(4), S(2), N(1)}.

and 3.618(1) Å for $[\{Rh(CO)_2(\mu\text{-mt})\}_2]$ **3** and $[\{Rh(CO)(PPh_3)(\mu\text{-mt})\}_2]$ **5** respectively.

The distortion of the Rh-N-C-S-Rh-N-C-S ring on formation of the trinuclear cations also results in a shorter distance between the centroids of the mutually inclined bridging rings. Compare, for example, $[\{Rh(CO)_2\}_3(\mu\text{-mt})_2]^+$ **10**$^+$ (3.291 Å) with $[\{Rh(CO)_2(\mu\text{-mt})\}_2]$ **3** (3.485 Å). However, that distance in $[\{Rh(cod)\}_3(\mu\text{-taz})_2]^+$ **9**$^+$ is much longer (3.704 Å) apparently as a consequence of the twisting of the ethyl group on one of the taz ligands so that its terminal methyl group is positioned between the two bridging heterocycles.

There is a notable difference in the effect of the ancillary ligands on the metal-metal distances in the di- and trinuclear species; steric effects seem more important for the dimers with the Rh···Rh distance varying, for example, from 3.049 Å in $[\{Rh(CO)_2(\mu\text{-mt})\}_2]$ **3** to 3.618 Å in $[\{Rh(CO)(PPh_3)(\mu\text{-mt})\}_2]$ **5** to 3.847 Å in $[\{Rh(cod)(\mu\text{-mt})\}_2]$ **1**. By contrast, the distance between terminal and central rhodium atoms in the trinuclear cations only varies from 3.034 to 3.292 Å {*e.g.* compare $[\{Rh(CO)_2\}_3(\mu\text{-mt})_2]^+$ **10**$^+$ (3.055 Å) with $[\{Rh(CO)(PPh_3)\}_3(\mu\text{-mt})_2]^+$ **12**$^+$ (3.077 and 3.034 Å)} and that between the terminal rhodium atoms varies between 5.06 to 5.20 Å. {The latter distance is actually marginally longer

 

in the unhindered hexacarbonyl $[\{Rh(CO)_2\}_3(\mu\text{-mt})_2]^+$ **10**$^+$ (5.076 Å) than in the tris(phosphine) $[\{Rh(CO)(PPh_3)\}_3(\mu\text{-mt})_2]^+$ **12**$^+$ (5.062 Å).}

In $[\{Rh(CO)(PPh_3)\}_3(\mu\text{-mt})_2]^+$ **12**$^+$ and $[\{Rh(CO)(PPh_3)\}_3(\mu\text{-taz})_2]^+$ **13**$^+$ all three phosphorus atoms are *trans* to sulfur resulting in each being chemically distinct (as observed by $^{31}$P NMR spectroscopy). The central phosphorus atom is, of course, unique but P(1) is *trans* to S(1), which is *trans* to CO, whereas P(2) is *trans* to S(2) which is *trans* to $PPh_3$. The structural study of **13**$^+$ also suggests an explanation for the differences observed in the proton and carbon chemical shifts (see above); the taz ring containing S(1) and N(4) is closer to the aromatic rings of two $PPh_3$ ligands, P(1)$Ph_3$ and P(3)$Ph_3$, which give a greater shielding effect than do the phenyl rings of the single P(2)$Ph_3$ ligand for the taz ring containing S(2) and N(1).

## Conclusions

In the solid state the *N*,*S*-bridged Rh(I) dimers $[\{RhLL'(\mu\text{-X})\}_2]$, [X = mt or taz, LL′ = cod, $(CO)_2$, $(CO)(PPh_3)$ or $\{P(OPh)_3\}_2$], prepared from $[\{RhLL'(\mu\text{-Cl})\}_2]$, HX and $NEt_3$, have an 'open book' geometry with two structural types resulting from differing conformations of the head-to-tail, eight-membered Rh-N-C-S-Rh-N-C-S ring. In $[\{Rh(cod)(\mu\text{-mt})\}_2]$ **1**, $[\{Rh(cod)(\mu\text{-taz})\}_2]$ **2**, $[\{Rh(CO)_2(\mu\text{-mt})\}_2]$ **3**, $[\{Rh(CO)(PPh_3)(\mu\text{-mt})\}_2]$ **5** and $[\{Rh(CO)(PPh_3)(\mu\text{-taz})\}_2]$ **6**, with rhodium-eclipsed geometries, the extent of the mutual twisting and tilting of the two rhodium square planes depends on the nature of the ancillary ligands, the Rh ··· Rh distance varying from 3.05 to 3.85 Å. The least hindered of these complexes, the dark blue-brown dicarbonyl **3**, uniquely shows intermolecular mt ring–ring stacking. By contrast, the steric bulk of the four $P(OPh)_3$ ligands of $[\{Rh[P(OPh)_3]_2(\mu\text{-taz})\}_2]$ **7** leads to a sulfur-eclipsed conformation, with a Rh ··· Rh distance of 4.97 Å.

Chemical oxidation of $[\{RhLL'(\mu\text{-X})\}_2]$ with $[Fe(\eta\text{-}C_5H_5)_2]^+$ or $[Fe(\eta\text{-}C_5H_4COMe)(\eta\text{-}C_5H_5)]^+$ provides a new route to the complexes $[(RhLL')_3(\mu\text{-mt})_2]^+$; oxidative bridge-splitting of the dimer liberates the monomeric rhodium(I) fragment $[RhLL']^+$ which then reacts with $[\{RhLL'(\mu\text{-X})\}_2]$, probably in the sulfur-eclipsed conformation, to form the trinuclear Rh(I) cations. Substitution by cod of the carbonyl groups on the central rhodium metal of $[\{Rh(CO)_2\}_3(\mu\text{-mt})_2]^+$ **10**$^+$ gives $[Rh_3(CO)_4(cod)(\mu\text{-mt})_2]^+$ **14**$^+$.

The steric effects of L and L′ are less marked in the trinuclear cations with, for example, the $Rh_{terminal} \cdots Rh_{central}$ distances in the bent trirhodium skeletons of $[\{Rh(cod)\}_3(\mu\text{-taz})_2]^+$ **9**$^+$, $[\{Rh(CO)_2\}_3(\mu\text{-mt})_2]^+$ **10**$^+$, $[\{Rh(CO)(PPh_3)\}_3(\mu\text{-mt})_2]^+$ **12**$^+$, $[\{Rh(CO)(PPh_3)\}_3(\mu\text{-taz})_2]^+$ **13**$^+$ and $[Rh_3(CO)_4(cod)(\mu\text{-mt})_2]^+$ **14**$^+$ varying only from 3.03 to 3.29 Å.

## Experimental

The preparation, purification and reactions of the complexes described were carried out under an atmosphere of dry nitrogen, using solvents dried by Anhydrous Engineering double alumina or alumina/copper catalyst columns. All solvents were deoxygenated prior to use. Unless stated otherwise, complexes were purified using a mixture of two solvents. The impure solid was dissolved in the more polar solvent, the resulting solution was filtered and treated with the second solvent, and the mixture was then reduced in volume *in vacuo* to induce precipitation. Unless stated otherwise, the new complexes are stable under nitrogen and dissolve in solvents such as $CH_2Cl_2$, thf and, in the case of the binuclear species, toluene to give air-sensitive solutions. The compounds Htaz,[20] $[\{Rh(cod)(\mu\text{-Cl})\}_2]$,[21] $[\{Rh(CO)_2(\mu\text{-Cl})\}_2]$,[22] $[\{Rh(CO)(PPh_3)(\mu\text{-Cl})\}_2]$,[23] $[Fe(\eta\text{-}C_5H_5)_2][PF_6]$ and $[Fe(\eta\text{-}C_5H_4COMe)(\eta\text{-}C_5H_5)][BF_4]$[24] were prepared by published methods. Methimazole was purchased from Across Organics.

IR spectra in $CH_2Cl_2$ were recorded on a PerkinElmer Spectrum One FT-IR spectrometer. NMR spectra were recorded on a JEOL Eclipse 300 spectrometer, operating at 299.9 MHz for $^1$H, at 75.4 MHz for $^{13}$C and at 121.4 MHz for $^{31}$P, running JEOL Delta software. For $^1$H and $^{13}$C-{$^1$H} spectra, either $SiMe_4$ or residual protio solvent was used as an internal standard. For $^{31}$P-{$^1$H} spectra, 85% $H_3PO_4$ was used as an external standard.

Electrochemical studies were carried out using an EG&G model 273A potentiostat linked to a computer running either EG&G Model 270 Research Electrochemistry software or PAR Power Suite software, in conjunction with a three-electrode cell. The working electrode was a platinum disc (1.6 mm diameter) and the counter electrode a platinum wire. The reference was an aqueous saturated calomel electrode separated from the test solution by a fine porosity frit and an agar bridge saturated with KCl. Solutions in $CH_2Cl_2$ were $1.0 \times 10^{-3}$ mol dm$^{-3}$ in the test compound and 0.1 mol dm$^{-3}$ in $[NBu^n_4][PF_6]$ as the supporting electrolyte. Under the conditions used, $E^{o\prime}$ for the one-electron oxidation of $[Fe(\eta\text{-}C_5H_5)_2]$ and $[Fe(\eta\text{-}C_5Me_5)_2]$, added to the test solutions as internal calibrants, is 0.47 and –0.08 V respectively.

Microanalyses were carried out by the staff of the Microanalytical Service of the School of Chemistry, University of Bristol.

### Syntheses

**$[\{Rh(cod)(\mu\text{-taz})\}_2]$ 2.** Solid Htaz (190 mg, 1.33 mmol) was added to a stirred solution of $[\{Rh(cod)(\mu\text{-Cl})\}_2]$ (326 mg, 661 μmol) in toluene (60 cm$^3$); after 60 min, an excess (*ca.* 0.1 cm$^3$) of triethylamine was added. After a further 10 min the reaction mixture was filtered to remove solid $[NEt_3H]Cl$. The orange filtrate was concentrated *in vacuo* to *ca.* 5 cm$^3$ and then *n*-hexane was added to precipitate an orange solid which was dried *in vacuo*, yield 433 mg (93%).

**$[\{Rh(CO)_2(\mu\text{-mt})\}_2]$ 3.** A mixture of $[\{Rh(CO)_2(\mu\text{-Cl})\}_2]$ (500 mg, 1.29 mmol) and Hmt (295 mg, 2.58 mmol) in $CH_2Cl_2$ (50 cm$^3$) was stirred for 10 min and then excess $NEt_3$ (*ca.* 0.3 cm$^3$) was added. The resulting dark yellow-red solution was stirred for 15 min and then the solvent was removed *in vacuo*. The crude product, a dark blue-brown solid, was extracted into toluene (60 cm$^3$). The extract was filtered and then concentrated *in vacuo* to *ca.* 20 cm$^3$; addition of *n*-hexane precipitated a dark blue-brown solid which was further purified using $CH_2Cl_2$–*n*-hexane and dried *in vacuo*, yield 538 mg (77%).

The complexes $[\{Rh(cod)(\mu\text{-mt})\}_2]$ **1** and $[\{Rh(CO)(PPh_3)(\mu\text{-taz})\}_2]$ **6** were prepared similarly from $[\{Rh(cod)(\mu\text{-Cl})\}_2]$ and $[\{Rh(CO)(PPh_3)(\mu\text{-Cl})\}_2]$ respectively.

**$[\{Rh(CO)_2(\mu\text{-taz})\}_2]$ 4.** Carbon monoxide was bubbled through a solution of $[\{Rh(cod)(\mu\text{-taz})\}_2]$ **2** (138 mg, 195 μmol) in

**Table 7** Crystal and refinement data for [{Rh(cod)(μ-mt)}$_2$] **1**, [{Rh(cod)(μ-taz)}$_2$] **2**, [{Rh(CO)$_2$(μ-mt)}$_2$]·toluene **3**·toluene, [{Rh(CO)(PPh$_3$)(μ-mt)}$_2$] ·toluene **5**·toluene, [{Rh(CO)(PPh$_3$)(μ-taz)}$_2$] **6**, [{Rh[P(OPh)$_3$]$_2$(μ-taz)}$_2$] **7**, [{Rh(cod)}$_3$(μ-taz)$_2$][PF$_6$] **9**$^+$[PF$_6$]$^-$, [{Rh(CO)$_2$}$_3$(μ-mt)$_2$][BF$_4$] **10**$^+$[BF$_4$]$^-$, [{Rh(CO)(PPh$_3$)}$_3$(μ-mt)$_2$][BF$_4$]·CH$_2$Cl$_2$ **12**$^+$[BF$_4$]$^-$·CH$_2$Cl$_2$, [{Rh(CO)(PPh$_3$)}$_3$(μ-taz)$_2$][PF$_6$]·3CH$_2$Cl$_2$ **13**$^+$[PF$_6$]$^-$·3CH$_2$Cl$_2$ and [Rh$_3$(CO)$_4$(cod)(μ-mt)$_2$] [BF$_4$]·2CH$_2$Cl$_2$ **14**$^+$[BF$_4$]$^-$·2CH$_2$Cl$_2$

| | [{Rh(cod)(μ-mt)}$_2$] **1** | [{Rh(cod)(μ-taz)}$_2$] **2** | [{Rh(CO)$_2$(μ-mt)}$_2$]·toluene **3**·toluene | [{Rh(CO)(PPh$_3$)(μ-mt)}$_2$]·toluene **5**·toluene | [{Rh(CO)(PPh$_3$)(μ-taz)}$_2$] **6** | [{Rh{P(OPh)$_3$}$_2$(μ-taz)}$_2$] **7** | [{Rh(cod)}$_3$(μ-taz)$_2$][PF$_6$] **9**$^+$[PF$_6$]$^-$ | [{Rh(CO)$_2$}$_3$(μ-mt)$_2$][BF$_4$] **10**$^+$[BF$_4$]$^-$ | [{Rh(CO)(PPh$_3$)}$_3$(μ-mt)$_2$] [BF$_4$]·CH$_2$Cl$_2$ **12**$^+$[BF$_4$]$^-$·CH$_2$Cl$_2$ | [{Rh(CO)(PPh$_3$)}$_3$(μ-taz)$_2$][PF$_6$]·3CH$_2$Cl$_2$ **13**$^+$[PF$_6$]$^-$·3CH$_2$Cl$_2$ | [Rh$_3$(CO)$_4$(cod)(μ-mt)$_2$] [BF$_4$]·2CH$_2$Cl$_2$ **14**$^+$[BF$_4$]$^-$·2CH$_2$Cl$_2$ |
|---|---|---|---|---|---|---|---|---|---|---|---|
| Formula | $C_{24}H_{34}N_4Rh_2S_2$ | $C_{26}H_{40}N_6Rh_2S_2$ | $C_{19}H_{18}N_4O_4Rh_2S_2$ | $C_{53}H_{48}N_4O_2P_2Rh_2S_2$ | $C_{48}H_{46}N_6O_2P_2Rh_2S_2$ | $C_{83}H_{78}Cl_2N_6O_{12}P_4Rh_2S_2$ | $C_{34}H_{52}F_6N_6PRh_3S_2$ | $C_{14}H_{10}BF_4N_4O_6Rh_3S_2$ | $C_{66}H_{57}BCl_2F_4N_4O_3P_3Rh_3S_2$ | $C_{70}H_{67}Cl_6F_6N_6O_3P_4Rh_3S_2$ | $C_{22}H_{26}BCl_4F_4N_4O_4Rh_3S_2$ |
| $M$ | 648.49 | 706.58 | 636.31 | 1104.83 | 1070.79 | 1816.23 | 1062.64 | 789.92 | 1577.63 | 1863.73 | 1011.93 |
| Crystal system | Monoclinic | Monoclinic | Monoclinic | Monoclinic | Triclinic | Orthorhombic | Monoclinic | Monoclinic | Triclinic | Triclinic | Triclinic |
| Space group | $P2_1/c$ | $P2_1/c$ | $P2_1/c$ | $P2_1/c$ | $P$-1 | $P2_12_12$ | $P2_1/c$ | $C2/c$ | $P$-1 | $P$-1 | $P$-1 |
| $a$/Å | 11.141(2) | 18.847(4) | 6.742(1) | 18.748(4) | 11.370(2) | 16.991(3) | 8.302(2) | 16.757(3) | 11.982(1) | 11.673(2) | 10.979(2) |
| $b$/Å | 17.344(2) | 11.036(2) | 24.979(2) | 13.648(3) | 12.483(3) | 19.586(4) | 21.086(4) | 16.186(3) | 15.469(1) | 16.606(3) | 13.334(3) |
| $c$/Å | 12.795(2) | 30.704(6) | 14.086(1) | 21.383(4) | 17.364(4) | 11.929(2) | 21.516(4) | 11.502(2) | 18.572(1) | 21.794(4) | 13.909(3) |
| $\alpha$/° | 90 | 90 | 90 | 90 | 94.83(3) | 90 | 90 | 90 | 104.309(1) | 70.04(3) | 99.01(3) |
| $\beta$/° | 97.78(1) | 99.28(3) | 100.74(1) | 109.10(3) | 95.12(3) | 90 | 93.42(3) | 132.53(3) | 93.037(1) | 80.29(3) | 109.00(3) |
| $\gamma$/° | 90 | 90 | 90 | 90 | 102.30(3) | 90 | 90 | 90 | 99.896(1) | 76.75(3) | 114.02(3) |
| $T$/K | 173 | 100 | 173 | 100 | 100 | 100 | 173 | 100 | 173 | 173 | 100 |
| $V$/Å$^3$ | 2449.6(7) | 6303(2) | 2330.5(2) | 5169.9(18) | 2384.8(8) | 3969.9(14) | 3760.1(13) | 2298.8(8) | 3269.3(4) | 3846.2(13) | 1657.1(10) |
| $Z$ | 4 | 8 | 4 | 4 | 2 | 2 | 4 | 4 | 2 | 2 | 2 |
| $\mu$/mm$^{-1}$ | 1.538 | 1.204 | 1.627 | 0.824 | 0.891 | 0.683 | 1.521 | 2.382 | 1.028 | 1.046 | 1.984 |
| Reflections collected | 15353 | 70590 | 24595 | 58139 | 27239 | 45315 | 41346 | 7769 | 34532 | 43773 | 18603 |
| Independent reflections ($R_{int}$) | 5616 (0.0208) | 14455 (0.0828) | 5341 (0.0647) | 11852 (0.062) | 10898 (0.0492) | 9096 (0.0276) | 8591 (0.0526) | 2632 (0.0327) | 14840 (0.1034) | 17297 (0.0572) | 7519 (0.0426) |
| Final $R$ indices [$I > 2\sigma(I)$]: $R1$,$wR2$ | 0.0223, 0.0567 | 0.0676, 0.1407 | 0.0402, 0.0984 | 0.0270, 0.0658 | 0.0423, 0.0933 | 0.0236, 0.0678 | 0.0384, 0.0864 | 0.0540, 0.1175 | 0.0628, 0.1622 | 0.0516, 0.1235 | 0.0810, 0.2188 |

$CH_2Cl_2$ (35 $cm^3$) for *ca.* 15 min. The orange-red solution was then concentrated *in vacuo* and *n*-hexane added to precipitate a purple air-sensitive solid which was isolated by filtration and dried *in vacuo*, yield 75 mg (64%).

**[{Rh(CO)(PPh$_3$)(μ-mt)}$_2$] 5.** To a solution of [{Rh(CO)$_2$(μ-mt)}$_2$] **3** (50 mg, 90 μmol) in toluene (40 $cm^3$) was added $PPh_3$ (49 mg, 0.18 mmol). The yellow solution was filtered after 30 min and then concentrated *in vacuo* to *ca.* 20 $cm^3$; addition of *n*-hexane precipitated a yellow solid which was dried *in vacuo*, yield 30 mg (32%).

**[{Rh[P(OPh)$_3$]$_2$(μ-taz)}$_2$] 7.** An excess of $P(OPh)_3$ (*ca.* 0.1 $cm^3$) was added to [{Rh(CO)$_2$(μ-taz)}$_2$] **4**, generated *in situ* by adding an excess of $NEt_3$ (*ca.* 0.1 $cm^3$) to a mixture of [{Rh(CO)$_2$(μ-Cl)}$_2$] (210 mg, 0.54 mmol) and Htaz (155 mg,1,08 mmol) in $CH_2Cl_2$ (40 $cm^3$). After stirring the mixture for 80 min, the solvent was removed *in vacuo* to give a brown solid residue which was extracted into toluene (*ca.* 40 $cm^3$) and then concentrated *in vacuo* to *ca*. 5 $cm^3$. Addition of *n*-hexane precipitated a pale brown solid which was isolated by filtration. A concentrated $CH_2Cl_2$ solution of the solid was then added to a silica gel/$CH_2Cl_2$ chromatography column. Elution with $CH_2Cl_2$ gave a yellow solution which was concentrated *in vacuo* to *ca*. 5 $cm^3$; addition of *n*-hexane and cooling the mixture to −10 °C gave a pale yellow solid which was dried *in vacuo*, yield 204 mg (22%).

**[{Rh(cod)}$_3$(μ-taz)}$_2$][PF$_6$] 9$^+$[PF$_6$]$^-$.** To an orange solution of [{Rh(cod)(μ-taz)}$_2$] **2** (159 mg, 225 μmol) in $CH_2Cl_2$ (45 $cm^3$) was added [Fe(η-$C_5H_5$)$_2$][$PF_6$] (153 mg, 462 μmol). After 45 min the solvent was removed from the red-black solution *in vacuo* and the crude product washed with 3 × 20 $cm^3$ portions of *n*-hexane. The solid was dissolved in *ca.* 2 $cm^3$ $CH_2Cl_2$ and then passed through a short alumina/$CH_2Cl_2$ column. The red $CH_2Cl_2$ eluate was concentrated *in vacuo* to *ca*. 5 $cm^3$ and, after adding *n*-hexane and cooling the mixture to −10 °C, a dark red solid was precipitated, yield 78 mg (49% based on rhodium).

The compound [{Rh(CO)(PPh$_3$)}$_3$(μ-taz)}$_2$][$PF_6$] **13**$^+$[$PF_6$]$^-$ was prepared similarly from **6**, as were [{Rh(cod)}$_3$(μ-mt)$_2$][$BF_4$] **8**$^+$[$BF_4$]$^-$, [{Rh(CO)$_2$}$_3$(μ-mt)$_2$][$BF_4$] **10**$^+$[$BF_4$]$^-$ and [{Rh(CO)(PPh$_3$)}$_3$(μ-mt)$_2$][$BF_4$] **12**$^+$[$BF_4$]$^-$ (from **1**, **3**, and **5** respectively) but by using [Fe(η-$C_5H_4$COMe)(η-$C_5H_5$)][$BF_4$] as the oxidant.

**[{Rh(CO)$_2$}$_3$(μ-taz)}$_2$][PF$_6$] 11$^+$[PF$_6$]$^-$.** Carbon monoxide was bubbled through a solution of [{Rh(cod)}$_3$(μ-taz)$_2$][$PF_6$] **9**$^+$[$PF_6$]$^-$ (84 mg, 79 μmol) in $CH_2Cl_2$ (30 $cm^3$) for *ca*. 30 min. The red-black solution was then concentrated *in vacuo* and *n*-hexane added to precipitate a dark purple air-sensitive solid which was isolated by filtration and dried *in vacuo*, yield 46 mg (64%).

**[Rh$_3$(CO)$_4$(cod)(μ-mt)$_2$][BF$_4$] 14$^+$[BF$_4$]$^-$.** Carbon monoxide was bubbled through a solution of [{Rh(cod)}$_3$(μ-mt)$_2$][$BF_4$] **8**$^+$[$BF_4$]$^-$ (40 mg, 42.3 μmol) in $CH_2Cl_2$ (20 $cm^3$) for 15 min. The flow of CO was stopped and after 5 min the solution was concentrated *in vacuo* before *n*-hexane (40 $cm^3$) was added. The mixture was stored overnight at −10 °C to give purple crystals which were dried *in vacuo*, yield 31 mg (80%).

### Structure determinations

Many of the details of the structure analyses of [{Rh(cod)(μ-mt)}$_2$] **1**, [{Rh(cod)(μ-taz)}$_2$] **2**, [{Rh(CO)$_2$(μ-mt)}$_2$]·toluene **3**·toluene, [{Rh(CO)(PPh$_3$)(μ-mt)}$_2$]·toluene **5**·toluene, [{Rh(CO)(PPh$_3$)(μ-taz)}$_2$] **6**, [{Rh[P(OPh)$_3$]$_2$(μ-taz)}$_2$] **7**, [{Rh(cod)}$_3$(μ-taz)$_2$][$PF_6$] **9**$^+$[$PF_6$]$^-$, [{Rh(CO)$_2$}$_3$(μ-mt)$_2$][$BF_4$] **10**$^+$[$BF_4$]$^-$, [{Rh(CO)(PPh$_3$)}$_3$(μ-mt)$_2$][$BF_4$]·$CH_2Cl_2$ **12**$^+$[$BF_4$]$^-$·$CH_2Cl_2$, [{Rh(CO)(PPh$_3$)}$_3$(μ-taz)$_2$][$PF_6$]·3$CH_2Cl_2$ **13**$^+$[$PF_6$]$^-$·3$CH_2Cl_2$ and [$Rh_3$(CO)$_4$(cod)(μ-mt)$_2$] [$BF_4$]·2$CH_2Cl_2$ **14**$^+$[$BF_4$]$^-$·2$CH_2Cl_2$ are given in Table 7.

X-ray diffraction experiments on **1**, **3**·toluene, **9**$^+$[$PF_6$]$^-$, **12**$^+$[$BF_4$]$^-$·$CH_2Cl_2$ and **13**$^+$[$PF_6$]$^-$·3$CH_2Cl_2$ were carried out on a Bruker SMART diffractometer at 173 K. Similar experiments on **2**, **5**·toluene, **6**, **7**, **10**$^+$[$BF_4$]$^-$ and **14**$^+$[$BF_4$]$^-$·2$CH_2Cl_2$ were carried out on a Bruker APEX diffractometer at 100 K. All used Mo-$K_\alpha$ X-radiation ($\lambda$ = 0.71073 Å). All data were collected using a CCD area-detector, from a single crystal coated in paraffin oil or high-vacuum grease mounted on a glass fibre. Intensities were integrated[25] from several series of exposures, each exposure covering 0.3° in $\omega$. Absorption corrections were based on equivalent reflections using *SADABS*,[26] and structures were refined against all $F_o^2$ data with hydrogen atoms riding in calculated positions using *SHELXL*.[27] The residual electron density maps for **2**, **5** and **6** showed some peaks which could not be modelled satisfactorily; the data for these crystal structures were modelled with *PLATON*/*SQUEEZE*,[28] details for which may be found in the cif.†

There was some minor disorder pertaining to the anion or solvent molecules in four of the structures for which restraints were imposed in order to ensure smooth refinement. In **1**, the cyclooctadiene ligand was disordered over two positions, which converged to a 0.67 : 0.33 ratio. In **10**$^+$[$BF_4$]$^-$, three of the fluorine atoms in the [$BF_4$]$^-$ anion are disordered over two positions, each with occupancy 0.5. In **13**$^+$[$PF_6$]$^-$·3$CH_2Cl_2$, the [$PF_6$]$^-$ anion and one of the $CH_2Cl_2$ molecules are disordered over two positions, each in a 0.65 : 0.35 ratio, and in **14**$^+$[$BF_4$]$^-$·2$CH_2Cl_2$ the [$BF_4$]$^-$ anion is disordered over two positions in a 0.65 : 0.35 ratio.

## Acknowledgements

We thank the EPSRC for postgraduate studentships (to R.J.B., M.J.L.-G., A.H. and T.R.-J) and Johnson Matthey for a generous loan of hydrated rhodium trichloride. We also acknowledge the use of the EPSRC's Chemical Database Service at Daresbury.[29]

## References

1 M. J. López-Gómez, N. G. Connelly, M. F. Haddow, A. Hamilton and A. G. Orpen, *Dalton Trans.*, 2010, **39**, 5221.
2 R. J. Blagg, J. P. H. Charmant, N. G. Connelly, M. F. Haddow and A. G. Orpen, *Chem. Commun.*, 2006, 2350; R. J. Blagg, C. J. Adams, J. P. H. Charmant, N. G. Connelly, M. F. Haddow, A. Hamilton, J. Knight, A. G. Orpen and B. M. Ridgway, *Dalton Trans.*, 2009, 8724.
3 M. A. Ciriano, F. Viguri, J. J. Perez-Torrente, F. J. Lahoz, L. A. Oro, A. Tiripicchio and M. Tiripicchio-Camellini, *J. Chem. Soc., Dalton Trans.*, 1989, 25.
4 M. A. Ciriano, J. J. Perez-Torrente, F. Viguri, F. J. Lahoz, L. A. Oro, A. Tiripicchio and M. Tiripicchio-Camellini, *J. Chem. Soc., Dalton Trans.*, 1990, 1493.
5 T. Sielisch and M. Cowie, *Organometallics*, 1988, **7**, 707.
6 L. Dahlenburg and M. Kühnlein, *Eur. J. Inorg. Chem.*, 2000, 2117.

7 A. J. Deeming, M. N. N. Meah, H. M. Dawes and M. B. Hursthouse, *J. Organomet. Chem.*, 1986, **299**, C25.
8 M. A. Ciriano, J. J. Pérez-Torrente, L. A. Oro, A. Tiripicchio and M. Tiripicchio-Camellini, *J. Chem. Soc., Dalton Trans.*, 1991, 255.
9 M. A. Ciriano, J. J. Pérez-Torrente, F. J. Lahoz and L. A. Oro, *J. Organomet. Chem.*, 1993, **455**, 225.
10 M. A. Ciriano, S. Sebastián, L. A. Oro, A. Tiripicchio, M. Tiripicchio Camellini and F. J. Lahoz, *Angew. Chem., Int. Ed. Engl.*, 1988, **27**, 402.
11 M. Cowie and T. Sielisch, *J. Organomet. Chem.*, 1988, **348**, 241.
12 C. Tejel, B. E. Villarroya, M. A. Ciriano, L. A. Oro, M. Lanfranchi, A. Tiripicchio and M. Tiripicchio-Camellini, *Inorg. Chem.*, 1996, **35**, 4360.
13 C. Tejel, B. E. Villarroya, M. A. Ciriano, A. J. Edwards, F. J. Lahoz, L. A. Oro, M. Lanfranchi, A. Tiripicchio and M. Tiripicchio-Camellini, *Inorg. Chem.*, 1998, **37**, 3954.
14 J. J. Pérez-Torrente, M. A. Casado, M. A. Ciriano, F. J. Lahoz and L. A. Oro, *Inorg. Chem.*, 1996, **35**, 1782.
15 N. G. Connelly, C. J. Finn, M. J. Freeman, A. G. Orpen and J. Stirling, *J. Chem. Soc., Chem. Commun.*, 1984, 1025; N. G. Connelly, G. Garcia, M. Gilbert and J. S. Stirling, *J. Chem. Soc., Dalton Trans.*, 1987, 1403; D. C. Boyd, N. G. Connelly, G. Garcia Herbosa, M. G. Hill, K. R. Mann, C. Mealli, A. G. Orpen, K. E. Richardson and P. H. Rieger, *Inorg. Chem.*, 1994, **33**, 960.
16 A. Gajete-Perez and N. G. Connelly, unpublished results.
17 R. Usón, L. A. Oro, M. A. Ciriano, M. T. Pinillos, A. Tiripicchio and M. Tiripicchio-Camellini, *J. Organomet. Chem.*, 1981, **205**, 247.
18 R. J. Blagg, N. G. Connelly, M. F. Haddow, A. Hamilton, M. Lusi, A. G. Orpen and B. M. Ridgway, *Dalton Trans.*, 2010, **39**, 11616.
19 N. G. Connelly, P. R. G. Davis, E. E. Harry, P. Klangsinsirikul and M. Venter, *J. Chem. Soc., Dalton Trans.*, 2000, 2273.
20 M. Careri, L. Elviri, M. Lanfranchi, L. Marchiò, C. Mora and M. A. Pellinghelli, *Inorg. Chem.*, 2003, **42**, 2109.
21 G. Giordano and R. H. Crabtree,, *Inorg. Synth.*, 1990, **28**, 88.
22 J. A. McCleverty and G. Wilkinson, *Inorg. Synth.*, 1990, **28**, 84.
23 D. F. Steele and T. A. Stephenson, *J. Chem. Soc., Dalton Trans.*, 1972, 2162.
24 N. G. Connelly and W. E. Geiger, *Chem. Rev.*, 1996, **96**, 877.
25 *SAINT integration software*, Bruker AXS, Madison, Wisconsin, 1998-2003.
26 G. M. Sheldrick, *SADABS, Versions 2.03 (2001) and 2.10 (2003)*, Bruker AXS, Madison, Wisconsin.
27 G. M. Sheldrick, *Acta Crystallogr., Sect. A: Found. Crystallogr.*, 2008, **A64**, 112.
28 *PLATON/SQUEEZE* A. L. Spek, *J. Appl. Crystallogr.*, 2003, **36**, 7.
29 D. A. Fletcher, R. F. McMeeking and D. Parkin, *J. Chem. Inf. Comput. Sci.*, 1996, **36**, 746.


 